Chapter 6 Building Response 8/28/2022

In this chapter I will explore the nature of deformation and forces in buildings during earthquake shaking. Of course, buildings are complex connections of columns, beams, floors and walls, the study of which, deserves an entire course in structural engineering. However, as an introduction, it is instructive to investigate the nature of forces and deformations that would occur in a solid body whose properties are similar to the average properties of a building. I begin with a simple description of different types of buildings and comment on their characteristics in earthquake shaking. In general, I will characterize buildings with the following parameters (refer to Figure 6.1).

- Density is important because it is used to calculate inertial momentum. The density of buildings ranges from about 100 kg/m^3 (tall flexible frame buildings) to 200 kg/m^3 (stiff heavy shear wall buildings). Earthquake loads in buildings generally increase with the density of the building. These average densities are small compared to material densities because buildings are primarily air.
- Yield strength is maximum horizontal load that can be applied to a building. It is expressed in units of acceleration if the yield force is normalized by the weight of the building. While increasing yield strength is generally desirable, it usually comes with the penalty of increasing stiffness.
- Stiffness is the horizontal force distributed throughout a building divided by resulting lateral shear strain in the building (usually called drift). Maximum stresses in a building generally increases with stiffness, so making a building stiff can lead to high stresses. While low stiffness has advantages, decreasing stiffness usually comes with the penalties of increasing shear strains and decreasing yield strength.
- Ductility refers to the ratio of the horizontal shear strain at which a building collapses divided by the strain at which a building begins to strain inelastically. Increasing ductility is always desirable, but it usually comes with the penalty of increasing cost.

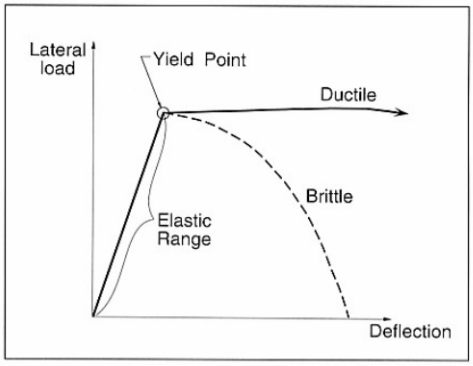

Figure 6.1 Idealized building response.

The following examples give some idea of different classes of buildings.

Concrete Shear-Wall Buildings

This is a common class of buildings that generally have at least some walls that consist of continuous slabs of concrete. These concrete walls are very resistant to in-plane shearing forces. Perpendicular shear walls are generally connected to each other through 1) the strong floor slabs, and 2) sometimes they are connected at corners of rooms. When a building consists of a rectangular concrete box with interior columns supporting the floor slab, then this is generally referred to as box/shear-wall construction. This type of construction is very common at Caltech. It has the advantage of very high yield strength. Furthermore, if the walls are properly reinforced, the ductility is also high. This type of construction has the disadvantages that it tends to lead to very stiff buildings with high average density. As we see later in the chapter, this can lead to high stresses in a building. It also has the disadvantage that the architecture of the building is fixed. That is, walls cannot be reconfigured once the building is constructed. Furthermore, because of their stiffness, it is impractical to build shear wall buildings taller than about 10 stories that also adequately resist earthquake loading.

Figure 6.2 shows two versions of the Olive View Hospital in the San Fernando Valley. The first version was a nonductile-concrete frame building that was completed just prior to its collapse in the 1971 San Fernando earthquake. The hospital was rebuilt as a shear wall structure (some of the shear walls were solid steel) and it experienced heavy shaking in the 1994 Northridge earthquake. In this case, there was no structural damage because of the very high yield strength of the building. I have heard structural engineers criticize this building for being "overbuilt." That said the overbuilt design ended up saving the County a lot of money during the violent shaking in 1994 (pga > 2 g recorded on the roof).

Figure 6.3 shows an example of a Japanese concrete shear-wall apartment building after the 1964 M 7.5 Niigata earthquake (see the figure caption). One-story concrete shear-wall buildings are quite common for construction of mini malls (e.g., 7-11 stores). They are simple to build (typically constructed with steel-reinforced concrete blocks) and they are inexpensive to build. They are extremely resilient to earthquake damage, but they are generally disdained by architects.

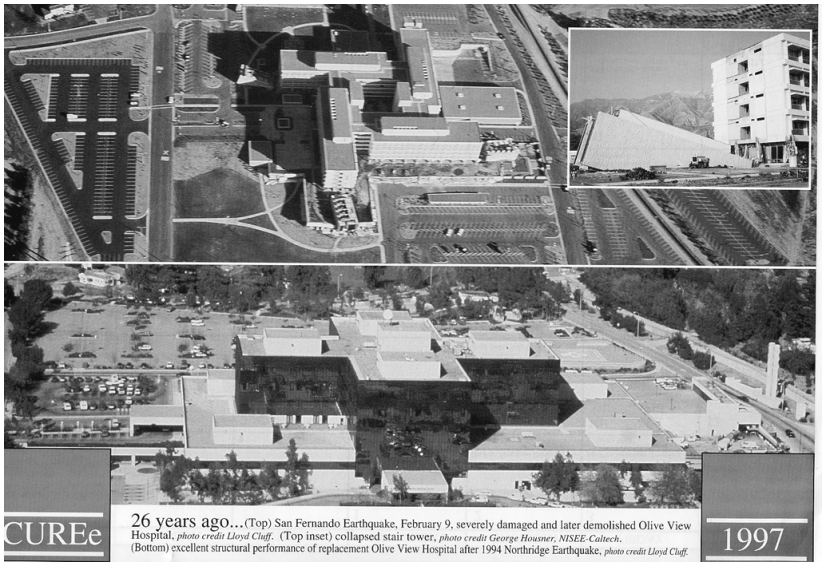

Figure 6.2 Two versions of the Olive View Hospital in the San Fernando Valley. The top picture shows the heavy damage that occurred to the first hospital (non-ductile concrete) in the 1971 M 6.7 San Fernando earthquake. The bottom picture shows the shear-wall structure that replaced the first one. This strong building had no structural damage as the result of the violent shaking in the 1994 M 6.7 Northridge earthquake.

Figure 6.3. Japanese concrete shear-wall apartment buildings after the 1964 M 7.2 Niigata earthquake. Despite the fact that the foundations of the buildings failed due to liquefaction, the building structures were undamaged and the buildings were later jacked back to an upright position and they were reoccupied.

Steel Moment Resisting Frame (SMRF) Buildings

This is a very common class of buildings, whose structural system generally consists of a rectangular lattice-work of columns and beams (the frame), together with the relatively rigid floor slabs, which are typically made of reinforced concrete. The columns and beams can be either mild steel (SMRF) or reinforced concrete. Figure 6.4 shows an example of a SMRF. These buildings are popular with many architects since they are 1) inexpensive, 2) office space can be easily reconfigured, and 3) they can be quite tall (The Library Towers in downtown Los Angeles is 80 stories high).

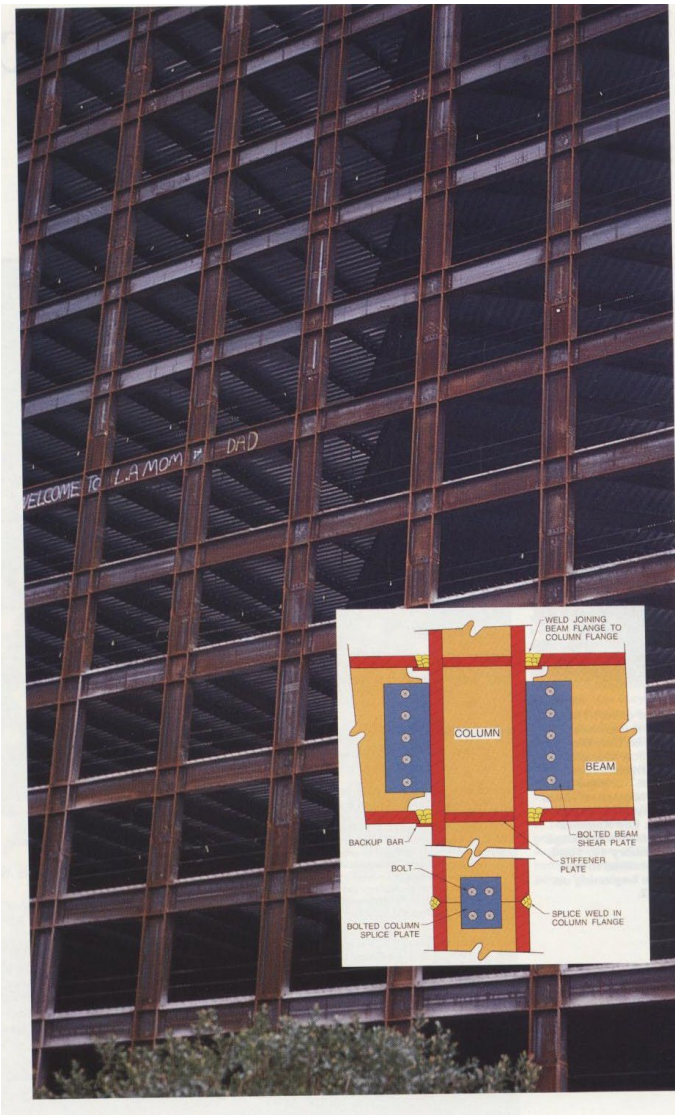

Figure 6.4. Example of a steel moment resisting frame. The connections between the beams and columns are typically welded (called a moment-resisting connection) to keep the elements perpendicular. Many of these critical connections were observed to fracture in the 1994 Northridge earthquake.

Figure 6.5 shows the basic physics of how an MRF resists lateral motion. As the frame is deflected horizontally, the beams and columns must bend if their connections remain perpendicular. Note that in typical US buildings, not all of the beam-column connections are moment resisting. Many of the interior connections are simple connections, which acts structurally more like a hinge. Although simple connections are adequate to support the weight of the floor slabs, they do not cause flexural bending of the beams. The moment-resisting beam-column connections are critical elements of a MRF since that is where the bending moment originates on a beam or column. It is critical that the MRF failure strength exceeds the flexural yield strength of the beams, since a building's ductility (high ductility is good) derives from the inelastic bending of beams (it's not good to inelastically bend columns since they carry gravitational loads).

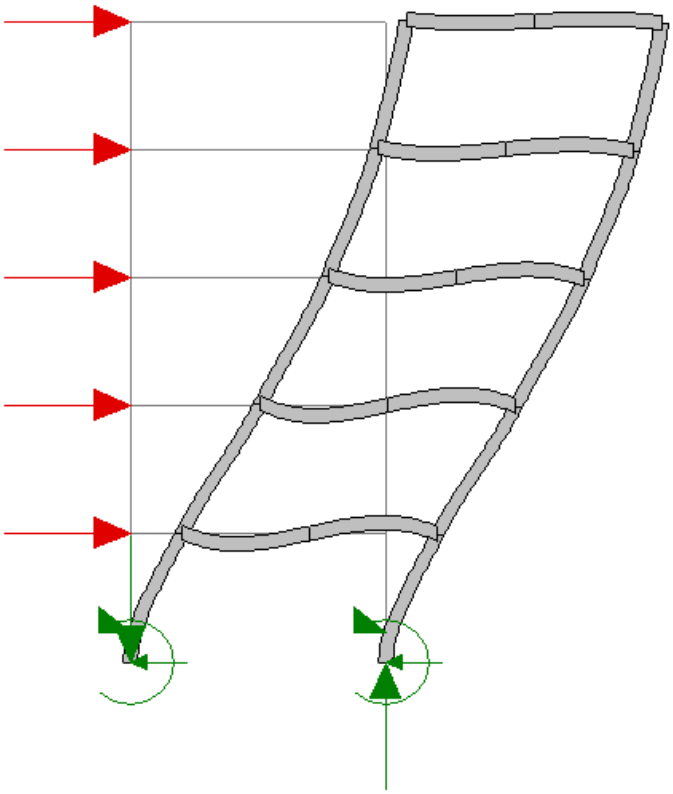

Figure 6.5. Cartoon showing how the flexural bending of beams and columns provides a resistance to lateral deformation for a moment-resisting frame structure. Note that only the connections on the exterior are moment frame connections, whereas the interior connection is a "simple" connection (unwelded) that acts more lie a structural hinge.

In the case of Steel MRF's, the moment resisting column-beam connections typically consist of welds between the flanges of the beams and columns (see Figure 6.4). These welded connections became popular in the 1960's since they are inexpensive to construct, and they were thought to have high strength. However, many of these welded connections fractured during the 1994 M 6.7 Northridge earthquake, so many of the

existing steel MRF's are not as ductile as designers thought when buildings were constructed. Figure 6.6 shows the design of moment-resisting steel beam-column connections that were used prior to the 1960's. For the connection to resist bending, it is critical that the flange of the beam (the top or bottom of the I-section) is firmly connected to the flange of a beam. For buildings with I-sections, that can only be accomplished at ½ of the connections (the connections where the beam flanges abut the column flanges). Prior to the 1960's, the flanges were usually connected to each other using either rivets or bolts.

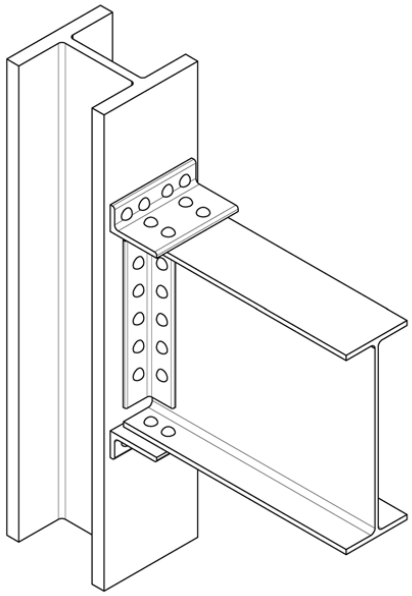

Figure 6.6. Schematic of a steel moment resisting connection that was common in older steel frame construction (pre 1960's). Connections used either rivets, or later, bolts._

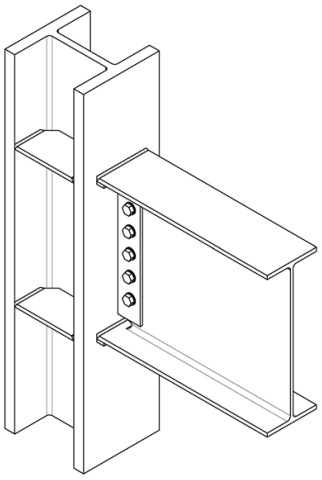

Figure 6.7. Schematic of a welded steel moment resisting connection that was common in steel frame construction (1960's to 1995). The web of the beam is simply connected using bolts. In contrast the flange of the beam is welded to the flange of the beam.

Beginning in the 1960's welded, steel, moment-resisting connections were introduced (Figure 6.7). It was believed that welded connections had a higher strength than either bolted or riveted connections. Importantly, welded connections were less expensive to construct than bolted connections.

The switch from bolted connections to welded connections was partially justified on the basis of lab testing of the relative strengths of bolted and welded connections. It was found that either type of connection was strong enough to cause ductile bending of a beam. That is the desired behavior. However, the lab testing was typically conducted using beams and columns that were significantly smaller than is seen for real high-rise buildings. That is, it would have been very expensive to build a lab test to bend the very large-size steel sections of real buildings. It was believed that the small-scale tests showed that the weld strength exceeded the bending strength.

Critical real-world tests of the performance of welded-steel moment-resisting-connections occurred during the 1994 Northridge and 1995 Kobe earthquakes. For the first time steel frame buildings were shaken strongly enough to cause inelastic structural response. In both cases, inspectors expected to observe plastically bent steel beams. To their horror, they did not find any bent steel, but they did find numerous examples of fractured welds (see Figure 6.8). At first, researchers suspected poor welding. However, when full-scale welded connections were tested in the lab, the full-scale tests showed that the welds fractured before there was enough force to bend the steel. This result happened even when the welds were "high quality."

Figure 6.8. Example of a welded steel connection that fractured in the 1994 Northridge Earthquake. Notice that the weld between the flanges experienced a tensile crack that extended across the web of the steel column. Prior to this earthquake, it was generally believe that mild structural steel would ductily bend, but that it would never fracture. .

It now seems that there is a size effect. That is, the forces required to fracture the welds did not scale with the cross-sectional area of the beams and columns. This size effect is complex and interesting. I will come back to the effect of size on the failure of materials in Chapter 8.

Steel moment-resisting connections were extensively modified in the latter 1990's and Figure 6.9 shows an example of a modern bolted and welded moment-resisting connection. Unfortunately, it is very expensive to "fix" brittle welds in existing buildings. Some have argued that it is only necessary to fix welds if they have previously failed in some past earthquakes, However, the fact that plastic yielding of steel was never observed for buildings in Kobe and Northridge indicates that all pre-1994 steel welds should be repaired since they are unlikely to survive the forces necessary to cause plastic bending of the beams.

Figure 6.9. Post Northridge Special Moment Resisting connection (welded and bolted) in one direction and simple connection in the orthogonal direction

While steel MRF's have the advantage that they are very flexible, that comes with the penalty that they have very low lateral strength. Figure 6.10 shows a **pushover analysis** (finite-element analysis by John Hall) of a 20-story SMRF building that meets the 1992 Uniform Building Code (UBC) code for California. This analysis included numerous nonlinear effects on the deformation of the steel, as well as also explicitly including the effect of how gravitational forces act on the building for large finite displacements. That is, when the drift of the building becomes large, then ever-increasing lateral loads are put on the building by gravity (kind of like the Tower of Pisa). This is known as the P-Δ effect and it is an important collapse mechanism for buildings.

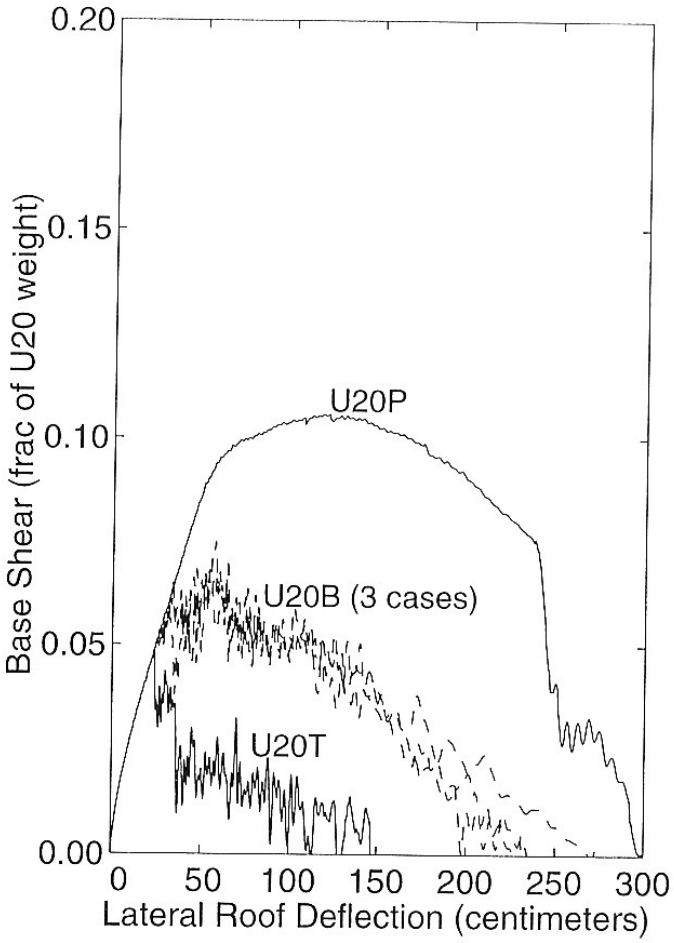

Figure 6.10 (from John Hall). Finite-element pushover analysis of a 20-story building that meets the 1992 US code standards for zone 4. P refers to the assumption that the moment frame connections do not fracture, B assumes that weld fractures occur randomly at stresses compatible with what was observe in the Northridge earthquake, and T assumes that the welds had even less fracture resistance.

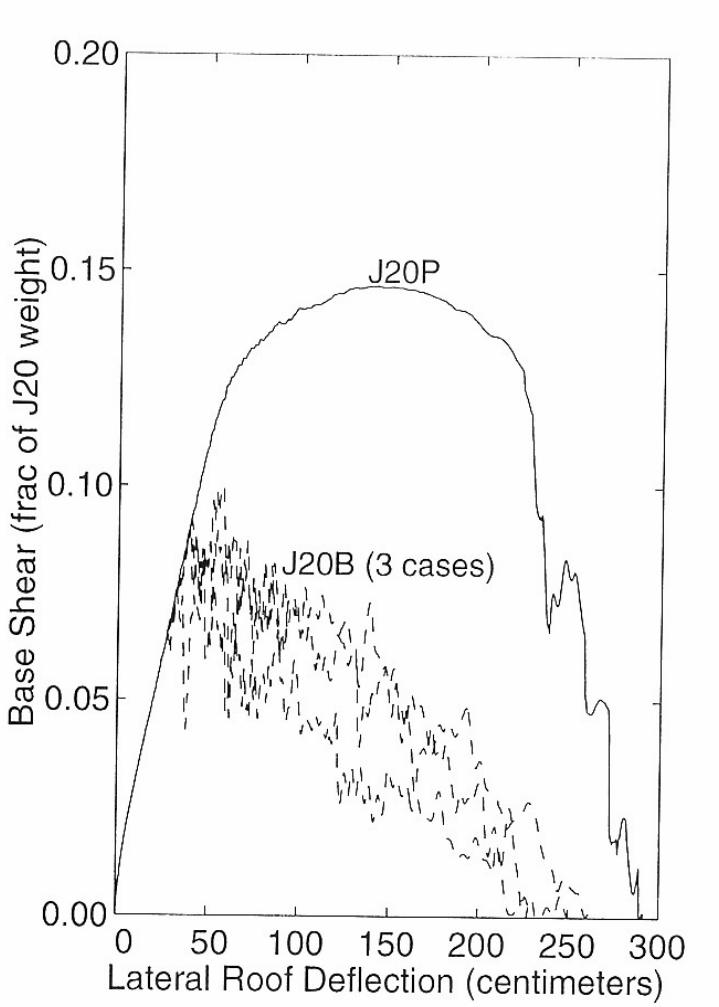

Figure 6.11. (from John Hall) Same as Figure 6.10., except for a 20-story steel frame building that meets Japanese codes in place in the 1990's. Notice the higher yield strength compared to the US building.

The curves U20P refer to a 20-story building that meets US 1992 zone 4 codes (highest code level), and for which the welded-moment resisting connections behave perfectly (no failures). The curve that is designated as B refers to allowing failure of the moment resisting connections assuming weld behavior consistent with observations in the 1994 Northridge earthquake. T refers to the assumption of "terrible" performance of the welds. Notice that weld failure significantly decreases both the yield strength and the ductility of the structure. Also notice that a horizontal force of only 7% of the weight of the building is necessary to push over a typical 20-story building in high seismic risk areas of the US.

Figure 6.11 shows a similar analysis, but it assumes that the building meets the building code in force in Japan in the 1990's. Japanese construction tends to put more emphasis on the yield strength of a structure, and it is common that all connections in a Japanese structure are moment-resisting connection (more costly than the US). Japanese steel buildings are commonly constructed with box section columns. This means that it is feasible to make all beam-column connections into moment-resisting connections.

As it turns out, the code required yield strength tends to increase as building height both increases and decreases from 20 stories. This is because design forces for wind loads increase as the building becomes taller, whereas design forces for earthquakes decrease as the building becomes taller (we'll visit this later). So buildings shorter than 20 stories are designed for earthquake loads and buildings taller than 20 stories are designed for wind loads. it is important that a building remain elastic for wind loads since wind loads are not oscillatory. If a building began to yield in a strong wind, then the force would remain and the building would just blow over. In contrast, it is assumed that earthquake loads are oscillatory; that is, the building deformation will reverse direction before the yielding becomes too large to survive P-Δ effects.

Figures 6.12 and 6.13 show the pushover analyses of 6-story steel moment resisting frame buildings for 1990's US and Japanese codes, respectively. Notice that the 6-story buildings are required to have a greater yield strength than the 20-story buildings.

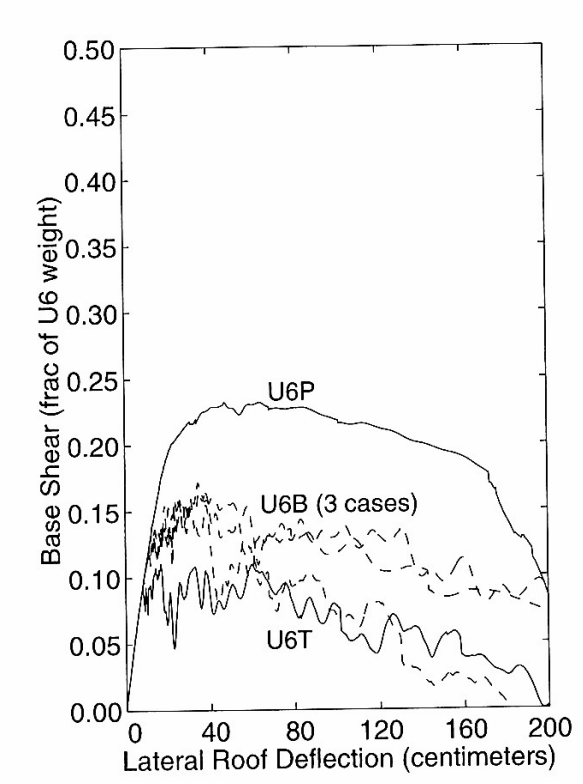

Figure 6.12 (from John Hall) Same as Figure 6.10, but for US-code, 6-story, steel-frame building.

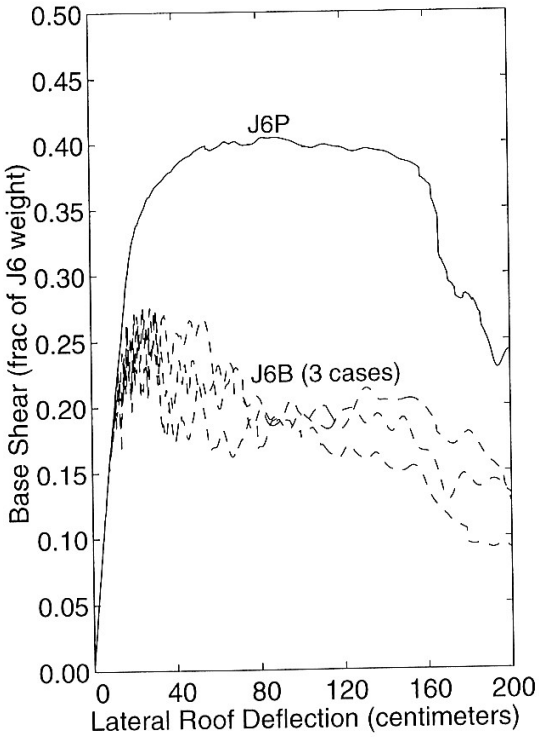

Figure 6.13 from John Hall. Same as Figure 6.10, but for Japanese-code, 6-story steel frame building

Concrete Moment-Resisting Frame Buildings

Moment resisting frame buildings can also be constructed with reinforced concrete beams and columns. Concrete mrf's have similar flexibility to steel mrf's and the code requirement for pushover yield strength is also similar. Both types of mrf's (steel and reinforce concrete) are required to have high ductility (approximately a factor of 10), but this is achieved in different ways with concrete. While steel is naturally ductile in tensional strain, unreinforced concrete is naturally brittle in tension (it is very strong in compression however). Although it is common to speak of the shear strength of the solid parts of the Earth, beams and columns generally carry longitudinal forces. In many cases, this can be axial tension or compression. In other cases, the element is subjected to bending forces (think of the forces in a diving board). In the case of bending, one side of the beam experienced tension while the opposite side experiences compression. In order to construct concrete beams that support bending (e.g., a beam supporting a floor), steel reinforcing bars (rebar) are run longitudinally in concrete beams in order to greatly increase the tensional strength and ductility. While longitudinal rebar is very important, it is not sufficient to make a beam adequately ductile. This was discovered through the inspection of reinforced concrete beams and columns that failed in the 1971 San Fernando earthquake. When a column experiences brittle failure, then the building collapsed vertically (referred to as a vertical collapse mechanism. An example of this type of failure is seen in Figure 6.14, which shows the failure of an 8-story concrete frame building in Mexico City from the M 7.2 1957 Acapulco earthquake. A more revealing photo of non-ductile failure of a concrete column is shown in Figure 6.15,

which shows a freeway bridge column that failed during the 1994 Northridge earthquake. Notice that the column originally fractured because of horizontal shear loads on the column. Although the failure was caused by shear stress in the column (this happens when the thickness of the column increases relative to its length), the failures actually consist of diagonal tensile cracks.

Once the concrete in the column cracked, the concrete fell away from the column and the remaining rebar buckled into a mushroom shape. This is an example of **non-ductile concrete** behavior. This deficiency was rectified by requiring spiral reinforcing bars that serves to confine the concrete to the beam, even if it is fractured. Figure 6.16 shows how a concrete column can continue to carry significant loads even though it has been strained well beyond its yield point. Unfortunately, this parking garage suffered significant collapse because the elements of the building were insufficiently connected to each other. That is, the reinforcing bars must adequately tie the different elements together.

Figure 6.14. Collapse of an 8-story non-ductile concrete moment-resisting frame building in Mexico City from the 1957 Acapulco earthquake.

Non-ductile concrete frame buildings are recognized as a class of particularly dangerous structures. They have the particularly bad combination of having a low yield stress combined with a low ductility (they're brittle). The tremendous loss of life in the 1999 Izmet Turkey earthquake was an example of non-ductile concrete frame failures. These failures are often very disastrous since the building often pancakes into a pile of floor slabs (referred to as a vertical collapse mechanism; very nasty). Many concrete moment

resisting frame buildings that were constructed in the United States prior to 1975 can also be classified as non-ductile concrete frames. Failures in the 1971 San Fernando earthquake resulted in a building code change in 1975 that significantly enhanced the ductility of buildings built after 1975. Unfortunately, repair of non-ductile concrete frame buildings is so expensive that there are very few ordinances that force a building owner to strengthen these buildings. Furthermore, most of the occupants of these buildings are not aware of the potential deficiencies of their building. Notably, the cities of Los Angeles and Santa Monica have passed laws that direct the Building Departments to publish lists of these buildings in those cities. Furthermore, the law directs owners to upgrade the buildings on a specified schedule that prioritizes actions according to the occupancy of the buildings. This work is not required to be completed for several decades.

It's important to distinguish concrete frame buildings from concrete shear wall buildings. That is, there are many old concrete shear wall buildings that are very resistant to failure in earthquakes, while most older concrete frame buildings may perform poorly in strong shaking.

Figure 6.15. Example of a nonductile concrete column failure on a freeway bridge during the 1994 Northridge earthquake. The column was fractured by horizontal shear, the concrete fell away, and then the weight of the bridge deck caused the rebar to buckle. This failure could have been avoided by adding more spiral reinforcing loops radially around the column to make it more ductile as is seen in Fig. 6.16.

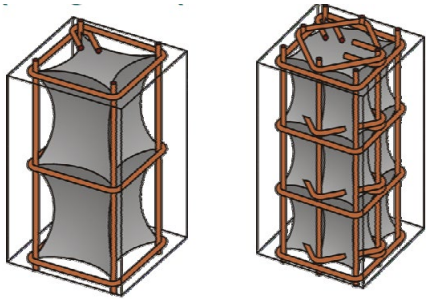

Figure 6.16. Schematic showing how the addition of additional circumferential reinforement increases the strength of concrete beams. This is referred to as “detailing.”

Figure 6.17. Example of ductile deformation of concrete columns from the 1994 Northridge earthquake. Adequate spiral reinforcing resulted in more ductile behavior than was shown in Figure 6.14. Unfortunately, the structure had other inadequacies that led to collapse as is shown in Figure 6.17.

Figure 6.18. Despite the ductile behavior of the concrete columns, this parking structure collapsed because the floor slabs were not adequately connected to the rest of the structure. That is, the beams and columns were ductile, but the connections between these elements were not.

Braced Frame Structures

The lateral yield strength of a building can be increased by adding diagonal braces to a structure, as is shown in Figure 6.19. Recall that the restoring force of a beam is primarily bending. In contrast the restoring force for a diagonal brace is primarily uniaxial compression (or tension, depending on the direction of the inter-story shearing). Beams are much stiffer in uniaxial deformation than they are in bending. In general, diagonal braces increase the pushover yield strength, while they also increase the overall stiffness of a building. That is, there is a trade-off between the desired trait of high strength and the undesired trait of high stiffness. Furthermore, it can be difficult to make a braced frame that has high ductility. This is because the use of large bracing elements tends to result in very stiff braces that apply very large loads to their connections with the structure, thereby concentrating damage at these connections. However, the use of small diameter bracing elements can end up with braces that tend to have ductile extension, but they buckle in compression. As a building undergoes cyclic loading, small braces become ineffectual, since they permanently extend for motions in one direction and then they buckle for motions in the opposite direction (see Figure 6.20). Caltech's Broad Center is one of the first buildings in the United States to use a new style of brace called an unbonded **bucking-restrained brace** (**brb**). This consists of a small diameter steel brace that is jacketed in a concrete liner. There is a lubricating element between the concrete and the steel. The concrete jacket prevents the brace from buckling in compression and hence this brace is ductile in both extension and compression. Figure 6.21 shows an example of Broad Center's unbonded buckling-restrained braces.

Figure 6.19. Example of a braced steel-frame.


Figure 6.20 Large braces are stiff and they put large loads into a frame, but small braces can buckle in compression.

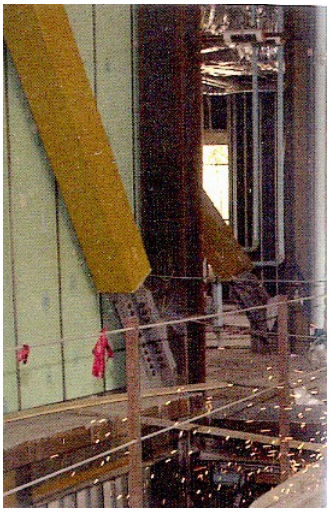

Unbonded Brace in the Broad Center

Figure 6.21. Broad Center bucking-restrained brace. The steel is ductile in tension and compression since it is jacketed by concrete (yellow) to prevent buckling in compression.

Base Isolated Structures

Throughout my career (starting in 1972), I have been asked about a common folk lore that buildings (especially high-rises) are built on rollers. I don't know where this story originated, but I have never encountered any buildings on rollers. That said, the use of base isolators has become ever more popular (especially in Japan) since they were first introduced in New Zealand in the 1980's. The idea is simple; introduce a highly flexible layer between the ground and a building. Loads to the building are dramatically reduced by concentrated shearing at the isolators. The first practical designs consisted of rubber disks placed between the foundation and the ground floor (see Fig. 6-22). In order to ensure that the rubber disks could carry the vertical loads from the weight of the building, stainless steel disks were molded into the isolators. In some cases, the disks also had a lead plug at their center to provide plastic damping. As you can see in Fig.6-22, the diameter of the isolator must be comparable to the largest lateral design displacement. The isolator of Fig 6-22 is relatively large (150 cm??) and it is intended to accommodate differential displacement of up to the size of the gap between the ground floor and the foundation. It is typical to construct a massive reinforced concrete box that is buried one story into the ground. The walls of the box prevent the differential motions from becoming so large that the isolator either tears or becomes gravitationally unstable. These walls are referred to as safety stops. Obviously, it is undesirable for the building to exceed the gap displacement in a real earthquake.

Figure 6-22. Base Isolated structure. The large black cylinder is one of many rubber/steel plate composite isolators that supports the weight of the building. The isolators are stiff in compression and flexible in shear. The concrete wall behind the engineer is the safety stop. The ground floor of the building is a massive reinforced concrete element that ensure that the ground floor moves as a rigid block.

There are some tradeoffs in the design of isolated buildings. It is desirable that the isolators can withstand large isolator drifts, which means that the isolators should have large diameters. However, such large rubber disks are surprisingly stiff and they come with the penalty that there is less isolation. Making the isolators taller (thicker) means that they are more flexible, but it also means that they become vulnerable to $P-\Delta$ instability.

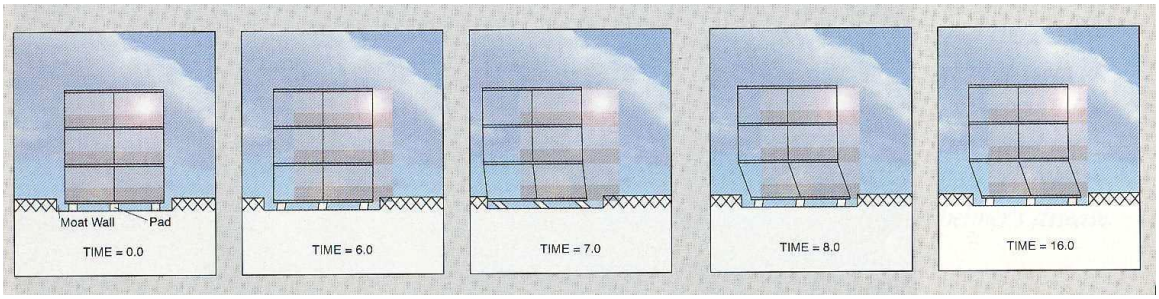

Figure 6-24. Simulation of a typical three-story base-isolated building in simulated near-source ground shaking from a hypothetical M 7.0 thrust earthquake.

The earliest generation of isolators typically had maximum differential displacements of about 35 cm. Following a paper by Heaton, Hall, Wald and Halling (1995, Response of high-rise and base-isolated buildings to a hypothetical M 7.0 blind thrust earthquake, Science, V 267, 206-211) that pointed out that near-source ground

motions from M > 7 earthquakes could exceed these design limits (see Figure 6-23), there was a move to increase the design drift of isolated buildings (see Figure 6-24).

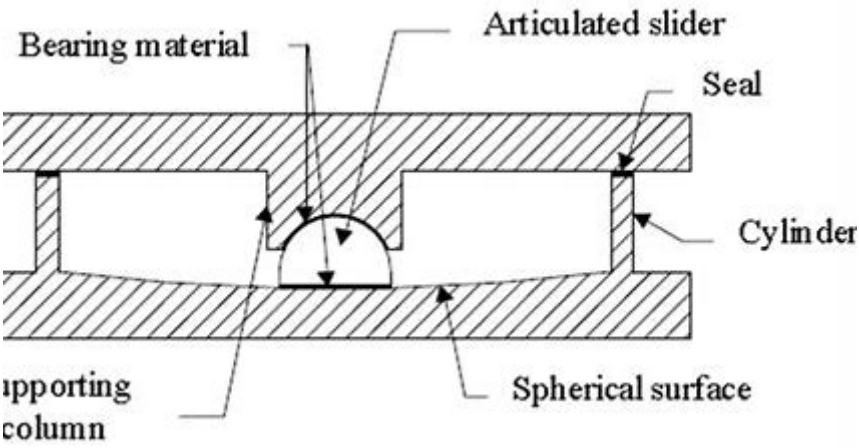

Figure 6-24. Schematic of a friction-pendulum bearing for base isolation. The sliding surfaces of the bearing are typically made of stainless steel that is coated to reduce sliding friction. The lateral restoring force for this system is gravity. The motion of the buildings is identical to that of a pendulum of the length of the radius of curvature of the spherical surface.

A new type of isolator was developed; a friction-pendulum isolator consists of a metal bearing that slides in a low-friction hemispherical cup, If the radius of curvature of the isolator is large, then the isolator can accommodate large differential displacements. Unlike the rubber base isolated buildings that only displace laterally, the motion of the pendulum-isolated building is the same as the motion of a pendulum whose length l_p is the radius of curvature of the isolator surface. Recall that the free period of a pendulum is $T_0 \approx 2\pi\sqrt{l_p/g} = 2.0\sqrt{l_p}$, where the pendulum length is in meters and the period is in seconds. Now the maximum lateral displacement of the pendulum is just $x_{\max} = l_p \sin\theta_{\max} \approx l_p\theta_{\max}$, where $\theta_{\max}$ is the maximum rotation of the pendulum in radians. Therefore, $T_0 \approx 2.0\sqrt{x_{\max}/\theta_{\max}}$. It is clear that the maximum rotation of the pendulum cannot be more than about 0.1 radians (1.57 radians corresponds to rotating the base to a vertical orientation). Assuming that $\theta_{\max} = 0.1$, then $T_0 \approx 6.3\sqrt{x_{\max}}$. This means that designing for large bearing displacements implies that the isolator system has large natural periods; an isolator maximum displacement of 1 m has a free period of about six seconds. As we will see in the next chapter, the maximum isolator displacement grows with isolator period for near-source ground motions in large earthquakes ($pgd \sim 10^{M/2}$). In reality, it is difficult to estimate the maximum isolator displacement that is expected at a given site. Nevertheless, it is currently common for

practicing engineers to ignore this issue when discussing base isolated buildings with the public and policy makers.

As long as the displacement of the ground is less than the maximum isolator displacement, then base isolated buildings are expected to have the benefit that the accelerations in the building will be substantially reduced compared to the ground acceleration. This is especially beneficial for historic buildings that are both fragile and socially important. In particular, the city halls of San Francisco, Los Angeles, Pasadena, and Salt Lake City have all been retrofitted with base isolation systems. Installing base-isolation in an existing building is remarkably expensive; it's probably less costly to build a new replica than it is to isolate an existing historic structure. Convincing political decision makers to commit public funds for these retrofits means that there is reluctance to admit that the systems will not survive large near-source ground motions.

Another benefit of base isolation is that the contents of isolated buildings (e.g., an expensive computer system) are less likely to be destroyed than for the same system in a traditional building since the peak accelerations in the building are typically reduced (that is, unless the building collides with its safety stops).

Wood-Frame Structures

Wood frame is the most common type of construction in California; most residences and many commercial structures are in this category. Since wood is thought of as a "flexible" material, you might think of a very flexible building when you think of a wood frame structure. This would be a mistake. In fact, most wood frame construction is extensively braced. Furthermore, continuous plywood panels, and sheetrock panels are typically fastened to either side of the wooden framing. Such walls may be best described as shear panels. These panels are geometrically connected into rectangular box shapes. In this sense, most wood frame construction might be better described as a shell type of structure. Another feature of wood frame construction is that the structure is relatively light; the dead load of the building is small compared with the weight of the contents (the live load). Because of the higher stiffness to mass ratio, wooden houses have high natural frequencies (typically 5 to 7 Hz).

Since it is not workable to construct houses that would crack their plaster walls when subjected to live loads (e.g., a piano, a graduation party), wood houses are also designed to have large yield stresses (compared to their weight). In fact, the pushover yield stress of most houses exceeds the weight of house. Furthermore, wood houses are designed to be stiff to limit the deflections caused by the live loads.

Wooden houses are also relatively ductile (the framing is redundant, and nails must be pulled out to disconnect elements). Because of these features (stiff, strong, and ductile), wood frame structures tend to perform very well in earthquakes. Despite the fact that these structures have been located in areas of violent shaking in past earthquakes,

collapse of these structures is exceedingly rare. Figure 6.22 shows the Turnagain Heights housing development (wood frame) following the 1964 Alaskan Earthquake. Despite the tremendous damage caused by a massive landslide beneath the development, the wood frame houses essentially remained intact.

1964 Alaska Earthquake, Turnagain Heights

Figure 6.22. Wood frame houses that rode through the massive landslide triggered by the 1964 Alaskan earthquake.

Quantification of ductility of wooden houses is a little tricky since it involves some understanding of how damage occurs. When wooden houses do yield, the damage is most often concentrated in the region between the foundation and the floor of the first story. In California, this region is often called a cripple wall. I don't want to get into the details of construction styles, so if you want to speak about any particular house, then you had better go to more detailed documents (like the wood retrofit report of the Calif. Earthquake Authority).

Unreinforced Masonry

In the earlier part of the 20th Century, many buildings were constructed of unreinforced brick; that is the exterior walls are several courses of brick and mortar, whereas the inner walls, floors, and roof are wood frame construction. The exterior brick walls in this type of construction tend to be heavy and brittle. That is, the walls cannot sustain tension. URM's have the undesirable characteristics that they are heavy, stiff, and quite brittle. The inadequacies of unreinforced masonry (URM) became obvious in the 1933 Long

Beach earthquake and many municipalities adopted building codes (between the mid 1930's and 1950, depending on the city) that required that these masonry construction buildings should be reinforced with steel. However, several cities have numerous examples of these historic structures. Following serious damage to URM's in the 1971 San Fernando earthquake, the cities of Los Angeles and Long Beach adopted controversial legislation that required that all URM should have some strengthening. At a minimum, this involved making stronger connections between the wooden floor trusses and the brick walls. This tends to decrease the bending moments on the base of the brick walls for out-of-plane shaking. Some buildings are also reinforced by building another structural system (often steel) within the building. Although strengthened URM's are an improvement on the pre-existing structures, there is a widely held belief that they are still lacking in strength and ductility. Despite their obvious shortcoming, the interior walls of URM's often prevent the catastrophic pancaking of the floors seen in non-ductile concrete frame buildings.

While almost all un-retrofitted masonry buildings constructed prior to 1930 are probably dangerous for even moderate levels of shaking, modern steel reinforced masonry buildings are thought to be among the most resilient structures available. That is, if you see a brick building, don't immediately assume that it is vulnerable. In California, most brick buildings constructed since 1950 are reinforced with steel.

Table 6.1 is a list of different types of buildings along with a general assessment of the structural characteristics of each type. This table is very generalized and qualitative. The actual characteristics of real buildings vary tremendously (caveat emptor).

Figure 6.23. Example of an unreinforced masonry building (URM).

Table 6.1 Qualitative summary of the characteristics of different building types.

Building type	stiffness	density	yield strength	ductility
Shear wall	high	high	high	medium
MRF	low	low	low	high
Braced MRF	medium	low	medium	high/medium
Nonductile concrete	medium	medium	low	low
Wooden house	high	low	high	high
URM	high	high	medium	low
Base Isolated	low	irrelevant	medium	varies greatly

Understanding Building Response

The next sections provide some methods for understanding the response of buildings in earthquakes. This is actually an enormous field of study and the analysis in these chapters is simply an introduction to the subject.

Building as a Rigid Block

Buildings are not rigid blocks! However, it is still instructive to investigate the forces in a rigid block that is subject to ground acceleration. This example has some application if the lowest natural frequency of the structure is high compared to the predominant frequency of the ground acceleration.

If both the building and the ground are considered to be rigid (how do you have earthquakes in a rigid earth?), then there are no waves and the problem can be solved by balancing force as follows. Consider a rigid building of height h , length and width w, and average density ρ that experiences a horizontal acceleration $\ddot{u}(t)$ as shown in Figure 6.24.

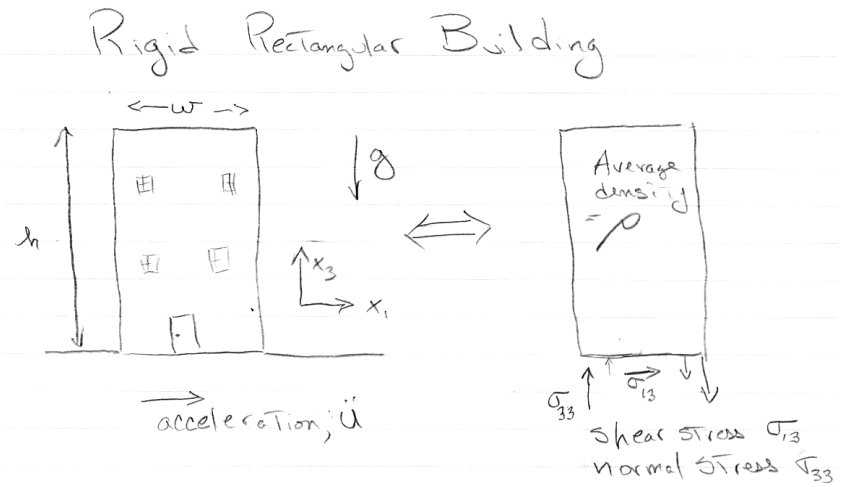

Figure 6.24. Forces acting on a rigid rectangular building that is sitting on a rigid earth. The cartoon on the right is known as a fre body diagram. There are both shear stresses to horizontally accelerate the building, and also a moment that is applied to the base to keep the building from rotating.

The total momentum of the building can be considered to be the sum of the translation of the center of mass of the building and also the rotational momentum of the building about an axis running through the center of the building. Since the ground is considered as rigid, the building cannot rotate and the translational momentum of the building is just

$$P_1(t) = \rho h w^2 \dot{u}(t) \tag{6.1}$$

where $P_1(t)$ is the momentum in the x_1 direction (that's all there is in this problem). The total horizontal force on the bottom of the building is

$$F_1(t) = \dot{P}_1(t) = \rho h w^2 \ddot{u}(t) \tag{6.2}$$

Therefore the shear stress on the bottom of the building is just the force divided by the cross sectional area, or

$$\sigma_{13}(t) = \rho h \ddot{u}(t) \tag{6.3}$$

So the shear stress at the bottom of a rigid building on a rigid earth just depends on the ground acceleration and the height of the building (assuming that the density is constant).

However, there is more to this simple problem. The shear stress at the bottom of the building would cause the building to rotate if there were no counteracting forces on the base of the building. That is the total moment applied to the base of the building must be zero, or

$$F_1(t)\frac{h}{2} - w\int_{-\frac{w}{2}}^{\frac{w}{2}} \left[\sigma_{33}(t, x_1) - \rho g h\right] x_1 dx_1 = 0 \tag{6.4}$$

where we assumed that the normal force on the base of the building consists of the weight of the building **plus** a moment that keeps the building form rotating. If we assume that the normal stress consists of constant compressional stress from the weight of the building $(\rho g h)$ plus another stress that varies linearly with distance along the base then

$$\sigma_{33}(x_1, t) = c(t) x_1 + \rho g h \qquad -w < x_1 < w \tag{6.5}$$

where $c(t)$ is now only a function of time. In this case

$$F_1(t)\frac{h}{2} - wc(t)\int_{-\frac{w}{2}}^{\frac{w}{2}} x_1^2 dx_1 = 0 \tag{6.6}$$

Substituting (6.2) into (6.6) and performing the integration yields

$$\frac{\rho h^2 w^2 \ddot{u}(t)}{2} - \frac{w^4}{12} c(t) = 0 \tag{6.7}$$

or

$$\sigma_{33}(x_1,t) = \rho g h + 6\rho\left(\frac{h}{w}\right)^2 x_1 \ddot{u}(t) \qquad -w < x_1 < w \tag{6.8}$$

Therefore the normal stresses at the outer edges of the building are

$$\begin{aligned}\sigma_{33}(x_1 = \pm w,t) &= \rho g h \pm 3\rho\left(\frac{h}{w}\right)^2 w\ddot{u}(t) \\ &= \rho h\left[g \pm 3\left(\frac{h}{w}\right)\ddot{u}(t)\right]\end{aligned} \tag{6.9}$$

There are cases where engineering materials fail easily in tension. Tensional stresses in our rigid building occur at the outer edge when

$$\ddot{u} > g\frac{w}{3h} \tag{6.10}$$

Therefore, rigid buildings that are tall compared with their width can result in tensional stresses in the exterior part of the building.

If we can approximately model the dynamics of a building with a rigid block, then the stresses in the building are determined by the **peak acceleration**. However, it has been long known that the peak accelerations observed in earthquakes are considerably larger than the nominal lateral strength of buildings that have survived those ground accelerations. As it turns out, the peak acceleration in most seismic records is strongly dependent on high-frequency parts of the motion (typically > 3 Hz), and the assumption that the building's fundamental frequencies are large compared to the ground acceleration does not apply.

Rigid Building on a Flexible Foundation (Rocking)

In this section I investigate what happens if we allow a rigid building to tilt due to flexibility of the foundation. This is not a very realistic problem to consider the ground to be far more flexible than the building, but it does illustrate how forces in the base of a building can be modified by the elasticity of the soil. This is called a **soil-structure interaction** (there are other effects that enter into this problem, but this is probably the most important). The problem is sketched in Figure 6.25. However, for the current discussion, we only ask the simpler question of how the rotation of the building changes the forces on the base of the building as compared with the previous section of this chapter.

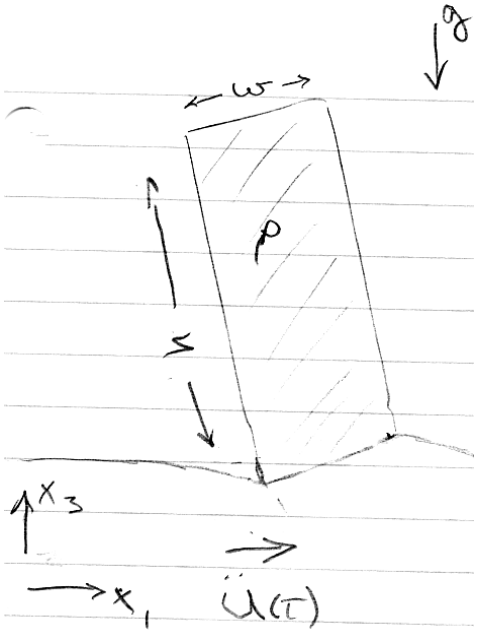

Figure 6.25 Cartoon of a rigid building on a flexible foundation

Solving for the forces in this problem involves separating the motion of the building into two parts; 1) the rectilinear motion of the center of mass of the building, and 2) the rotational motion about it axis of angular momentum. This decomposition is shown in Figure 6.26.

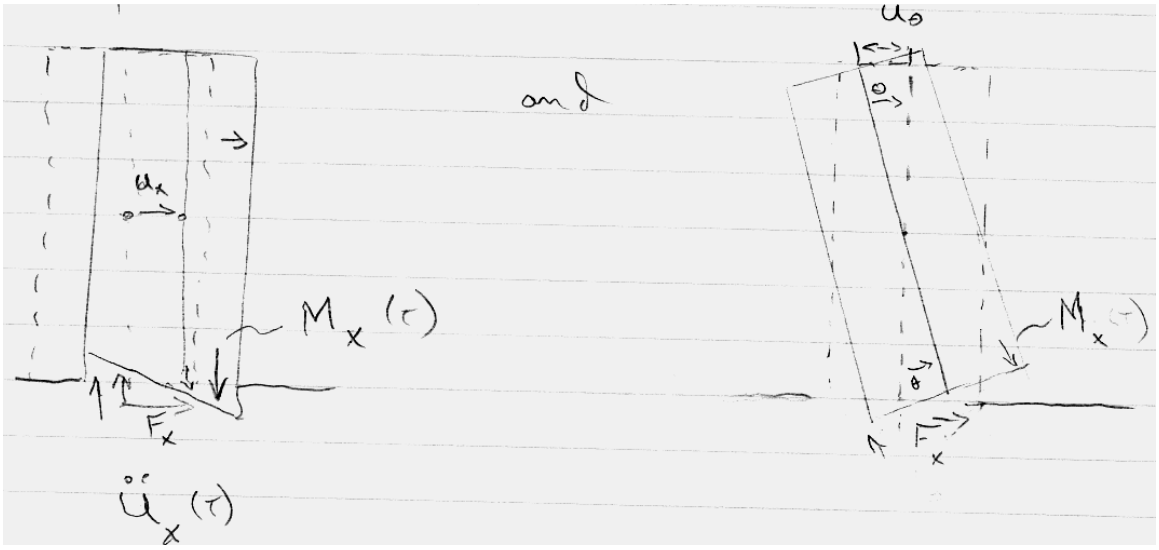

Figure 6.26 The motion of the rigid building can be viewed as the sum of a translation of the center of mass together with a rotation about the principal axis of inertia.

Let $u(t)$ be the motion of the base of the building in an inertial frame, $u_x(t)$ be the linear motion of the center of mass, and $u_\theta(t)$ be the motion of the base due to pure

rotation of the building about the center of rotation which is located at the midpoint of the building. Then

$$u(t) = u_x(t) + u_\theta(t) \tag{6.11}$$

and

$$\ddot{u}(t) = \ddot{u}_x(t) + \ddot{u}_\theta(t) \tag{6.12}$$

now

$$u_\theta(t) = \frac{h}{2}\sin\theta(t) \approx \frac{h}{2}\theta(t) \qquad \theta \ll \pi \tag{6.13}$$

then

$$\ddot{u}_\theta(t) \approx \frac{h}{2}\ddot{\theta}(t) \tag{6.14}$$

The force system on the base of the building can be considered to be the sum of the a horizontal force $F_1(t)$ (these are unbalanced) and a resisting moment $M(t)$ caused by the distribution of vertical stresses on the base of the building. The rectilinear momentum of the building $P(t)$ is just

$$P(t) = \rho w^2 \int_0^h \left(\dot{u}(t) - \frac{1}{2} x_3 \dot{\theta}(t) \right) dx_3 = m\left(\dot{u}(t) - \frac{1}{2} h\dot{\theta}(t) \right) \tag{6.15}$$

where $m = \rho h w^2$ is just the mass of the building. The force on the base of the building is then

$$F_1(t) = \dot{P}(t) = m\left(\ddot{u}(t) - \frac{1}{2} h\ddot{\theta}(t) \right) \tag{6.16}$$

The shear stress on the base of the building is then

$$\sigma_{13}(t) = \frac{F_1(t)}{w^2} = \frac{\dot{P}(t)}{w^2} = \rho h\left(\ddot{u}(t) - \frac{1}{2} h\ddot{\theta}(t) \right) \tag{6.17}$$

At this point, we do not yet know the shear stress, since we do not know $\theta(t)$. We can calculate the rotation of the building as follows,

$$M(t) + F_1(t)\frac{h}{2} = I\ddot{\theta}(t) \tag{6.18}$$

where

$$I = \frac{1}{12} m\left(h^2 + w^2 \right) \tag{6.19}$$

Combining (6.16), (6.17), and (6.19) yields

$$\ddot{\theta}(t) = \frac{12}{m\left(4h^2 + w^2 \right)}\left[M(t) + \frac{mh}{2}\ddot{u}(t) \right] \tag{6.20}$$

Now the moment at the base of the building is

$$M(t) = w \int_{-w/2}^{w/2} \sigma_{33}(t)\, x_1 dx_1 \tag{6.21}$$

If we assume that the normal stress is proportional to the vertical deflection, then

$$\sigma_{33}(t) = k\theta(t)x_1 \qquad -w/2 < x_1 < w/2 \tag{6.22}$$

where k is a type of stiffness with units of stress per unit of displacement (it differs from a regular spring constant, which has units of force per unit displacement) . Therefore,

$$M(t) = wk\theta(t)\int_{-w/2}^{w/2} x_1^2 dx_1 = \frac{1}{12}w^4 k\theta(t) \tag{6.23}$$

Combining (6.20) and (6.23) gives us the equation for a single degree of freedom forced oscillator

$$\ddot{\theta}(t) - \frac{kw^4}{m\left(4h^2+w^2\right)}\theta(t) = \frac{6h}{\left(4h^2+w^2\right)}\ddot{u}(t) \tag{6.24}$$

We immediately recognize that this is an un-damped forced linear oscillator with a natural period of

$$\omega_0 = w^2\sqrt{\frac{1}{4h^2+w^2}}\sqrt{\frac{k}{m}} \tag{6.25}$$

The full solution to this force oscillator is given in Chapter 1 (see equation 1.40 with damping equal to zero) as

$$\theta(t) = \frac{6h}{\left(4h^2+w^2\right)}\ddot{u}(t) * \left[H(t)\frac{\sin\omega_0 t}{\omega_0}\right] \tag{6.26}$$

While we have modeled the building as an un-damped sdof, the full solution to this problem is quite complex, since the oscillations of the building would excite waves in the elastic medium. The excitation of the waves would cause kinetic energy in the building to be radiated as wave energy into the surrounding medium. This would be a form of radiation damping of the oscillations of the building. Substituting (6.26) into (6.17) gives

$$\begin{aligned}\sigma_{13}(t) &= \rho h\left(\ddot{u}(t) - \frac{3h^2}{\left(4h^2+w^2\right)}\ddot{u}(t) * \frac{\partial^2}{\partial t^2}\left[H(t)\frac{\sin\omega_0 t}{\omega_0}\right]\right)\\ &= \rho h\ddot{u}(t) * \left(\delta(t) - \frac{3h^2}{w^2\sqrt{4h^2+w^2}}\sqrt{\frac{m}{k}}\frac{\partial^2}{\partial t^2}\left[H(t)\sin\omega_0 t\right]\right)\end{aligned} \tag{6.27}$$

We can also calculate the vertical compressive stresses at the outer edges of the building by substituting (6.26) into (6.22).

$$\begin{aligned}\sigma_{33}(t; x_1 = \pm w) &= \rho g h \pm kw\theta(t)\\ &= \rho g h \pm kw\frac{6h}{\left(4h^2+w^2\right)}\ddot{u}(t) * \left[H(t)\frac{\sin\omega_0 t}{\omega_0}\right]\\ &= \rho g h \pm \frac{6h}{w\sqrt{4h^2+w^2}}\sqrt{mk}\ddot{u}(t) * \left[H(t)\sin\omega_0 t\right]\end{aligned} \tag{6.28}$$

These are fairly complex relationships. However, we can get some idea of the effect of building tilting by investigating the initial response of the building to a impulse in acceleration, $\ddot{u}_{\max}$. In this case (6.27) becomes

$$\begin{aligned}
\sigma_{13}^{I}(t) &= \rho h \ddot{u}_{\max}\left(\delta(t)-\frac{3h^2}{\left(4h^2+w^2\right)}\delta(t)*\frac{\partial^2}{\partial t^2}\left[H(t)\frac{\sin\omega_0 t}{\omega_0}\right]\right)\\
&= \rho h \ddot{u}_{\max}\left(\delta(t)-\frac{3h^2}{\left(4h^2+w^2\right)}\frac{\partial}{\partial t}\left[\delta(t)\frac{\sin\omega_0 t}{\omega_0}+H(t)\cos\omega_0 t\right]\right)\\
&= \rho h \ddot{u}_{\max}\left(\delta(t)-\frac{3h^2}{\left(4h^2+w^2\right)}\left[\dot{\delta}(t)\frac{\sin\omega_0 t}{\omega_0}+2\delta(t)\cos\omega_0 t-H(t)\omega_0\sin\omega_0 t\right]\right)\\
&= \rho h \ddot{u}_{\max}\delta(t)\left(1-\frac{6h^2}{\left(4h^2+w^2\right)}\cos\omega_0 t\right)-\rho h \ddot{u}_{\max}H(t)\omega_0\sin\omega_0 t
\end{aligned} \tag{6.29}$$

Or we can write the shear response for an arbitrary acceleration as

$$\sigma_{13}^{I}(t) = \rho h \ddot{u}(t)\left(1-\frac{6h^2}{\left(4h^2+w^2\right)}\cos\omega_0 t\right)-\rho h \ddot{u}(t)*H(t)\omega_0\sin\omega_0 t \tag{6.30}$$

Therefore, **the shear maximum shear stress is decreased for a rocking building compared with a rigid base** (that is, for an impulse of acceleration). To fully understand the effect of this rocking, we would have to know the actual ground acceleration time history. If the ground motion was harmonic with the same period as the natural frequency of rocking, then the rocking building would resonate with the ground. If the duration of the ground motion was large enough, then the rocking building would develop even larger shears than the rigid building on the rigid foundation.

Notice that the acceleration impulse response for the outer edges of the building can be derived from (6.28), and is

$$\begin{aligned}
\sigma_{33}(t;x_1=\pm w) &= \rho g h \pm \frac{6h}{w\sqrt{4h^2+w^2}}\sqrt{mk}\,\ddot{u}_{\max}\delta(t)*\left[H(t)\sin\omega_0 t\right]\\
&= \rho g h \pm \frac{6h}{w\sqrt{4h^2+w^2}}\sqrt{mk}\,\ddot{u}(t)*\left[H(t)\sin\omega_0 t\right]
\end{aligned} \tag{6.31}$$

Notice that as $k \to 0$, a very, very flexible foundation, then

$$\sigma_{33}(t;x_1=\pm w) = \rho g h \qquad t \ll \omega_0 \tag{6.32}$$

That is, as the foundation becomes more flexible, the normal stresses on the columns from the overturning torque decrease. However, depending on the convolution term, there may be resonances and the compressive stresses may actually increase.

Building as a single-degree-of-freedom oscillator; Response Spectra

In the previous discussion, I discussed stresses in very stiff buildings that could be approximated as accelerating rigid blocks. Of course, buildings cannot be damaged if they do not deform. In reality, all buildings are flexible and more complex models are required to understand the vulnerabilities of flexible buildings. I now discuss the properties of a building modelled as a single-degree-of-freedom linear oscillator. This is identical to the problem of a simple seismometer that was discussed in Chapter 1 (Figure 1.1). I will shortly describe how this problem can be generalized to multi-degree-of-freedom linear oscillators. For now though, I will discuss the dynamics of a base-isolated building. In particular, I will assume that the building is approximately rigid and that it sits on a linearly elastic isolator that also has viscous (linear damping). Real isolators are nonlinear at large offsets, but I'll ignore that for now. Consider the sdof shown in Fig. 2.27.

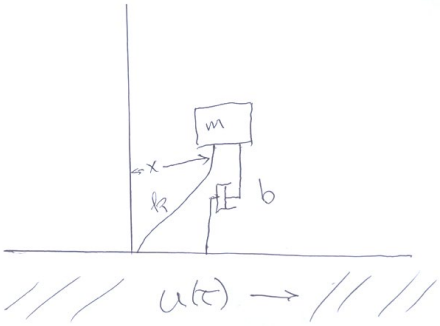

Figure 6.27 Building modeled as a single-degree-of-freedom damped oscillator. This model is useful for base-isolated buildings.

The system in Fig. 6.27 is exactly analogous to that shown in Fig. 1.1, except that the motions are horizontal. In particular, the ground moves horizontally with displacement $u(t)$; the horizontal motion $x(t)$ of a mass m is resisted by a spring of stiffness k; and there is a viscous damper that resists the relative velocity $\dot{x}$ of the mass with respect to the ground with force $-b\dot{x}$. The force on m is $-kx - b\dot{x}$ and the inertial force on m is $m(\ddot{u}+\ddot{x})$. The equation of motion of the system is then

$$m(\ddot{u}+\ddot{x})+b\dot{x}+kx=0 \tag{6.33}$$

which can be rewritten as

$$\ddot{x}+2\beta\dot{x}+\omega_0^2 x=-\ddot{u} \tag{6.34}$$

where $\omega_0=\sqrt{k/m}$ (the undamped natural frequency) and $\beta \equiv \dfrac{b}{2m}$ (the damping constant) which is related to the fraction of critical damping, ς, by $\beta = \omega_0 \varsigma$. It's important to recognize that $u(t)$ is motion with respect to an inertial frame, but $x(t)$ is a **noninertial coordinate.** However, $x(t)+u(t)$ is an inertial coordinate for the mass.

(6.34) can be easily solved using techniques in either the time domain, or alternatively, the frequency domain (see Chapter 1). For example. we can find the response to any ground motion by use of the convolution operator, which is defined as follows.

$$x(t) = \ddot{u}(t) * G(t) \equiv \int_{-\infty}^{\infty} \ddot{u}(\tau) G(t-\tau)\, d\tau \tag{6.35}$$

where

$$G(t) = H(t) \frac{1}{\omega_1} e^{-\beta t} \sin \omega_1 t \tag{6.36}$$

where

$$\omega_1 \equiv \sqrt{\omega_0^2 - \beta^2} \tag{6.37}$$

G(t) is a Green's function for this system; it is the response of the system to an impulse of ground acceleration. An impulse of acceleration induces a step in inertia, so this solution is identical to the transient response of the system with initial conditions of zero displacement and initial velocity of 1 m/s. The Green's function for 20% damping is shown in Figure 6.28.

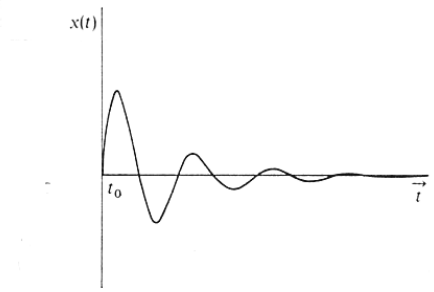

Figure 6.28. Response of a 20% damped sdof to an impulse of acceleration.

If there was no damping in the system, then the mass would move as a sinusoid indefinitely. Interestingly, the amplitude of the Fourier spectrum of x at ω_0 is identical to the amplitude of the steady state harmonic motion that persists after the ground acceleration is over.

When analyzing the dynamic response of elastic buildings, we are more interested in understanding the maximum deflections and forces than we are in the steady vibration. Furthermore, there is always dissipation (damping) in real structures. Suppose that we are interested in estimating the maximum isolator displacement for a base-isolated building. Then this is simply the **response spectral displacement**, which is defined as

$$S_d(\varsigma, \omega_0) \equiv \max_t \left[x(t; \varsigma, \omega_0) \right] \tag{6.38}$$

where ξ and ω_0 are the % critical damping and undamped natural frequency, respectively. Similarly, the **response spectral velocity** is defined as

$$S_v(\varsigma,\omega_0) \equiv \max_t\left[\dot{x}(t;\varsigma,\omega_0)\right] \tag{6.39}$$

and finally the **response spectral acceleration** is defined as

$$S_a(\varsigma,\omega_0) \equiv \max_t\left[\ddot{x}(t;\varsigma,\omega_0)+\ddot{u}\right] \tag{6.40}$$

Notice that spectral acceleration is defined with respect to the inertial coordinate $x+u$, which means that the response spectral acceleration measures the maximum force applied by the spring and damper (normalized by the mass). Figure 6.29 shows an example of response spectral velocity for a range of frequencies and damping. Response Spectra are ubiquitous in earthquake engineering, but please pay attention to the units. Tragically, even today it is common to see British units (inches and feet), which complicates any discussions between engineers and scientists. While any damping can be used, 5% damping is most commonly assumed; this is a pernicious mistake that I will discuss later.

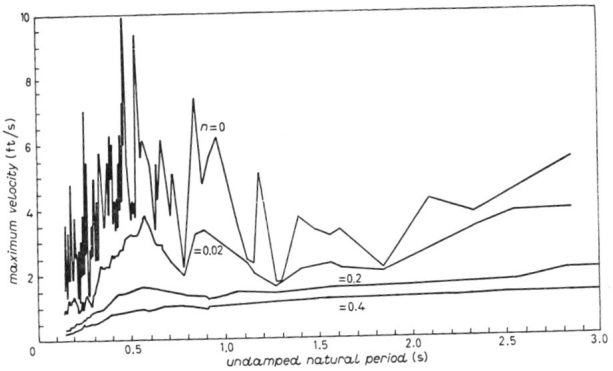

Figure 6.29. A very old figure (circa 1960's) showing response spectral velocities for a variety of damping (0, 2%, 20%, and 40%).

Response spectra are similar to Fourier spectra since they both characterize the amplitude as a function of frequency. Figure 6.30 compares the $S_v(\varsigma=0)$ (solid line) with the Fourier amplitude spectrum (dotted line) of a ground motion record. Notice that while theses spectra are similar, there are differences. In particular, the response spectrum is always greater than, or equal to the Fourier amplitude spectrum. That is because the response spectrum measures the maximum transient amplitude, while the Fourier spectrum measures the undamped steady state amplitude after the ground has stopped moving. The difference between these two spectra becomes more pronounced as the damping is increased. This difference is obvious in Figure 6.29, where it is seen that the response spectral amplitude decreases with damping.

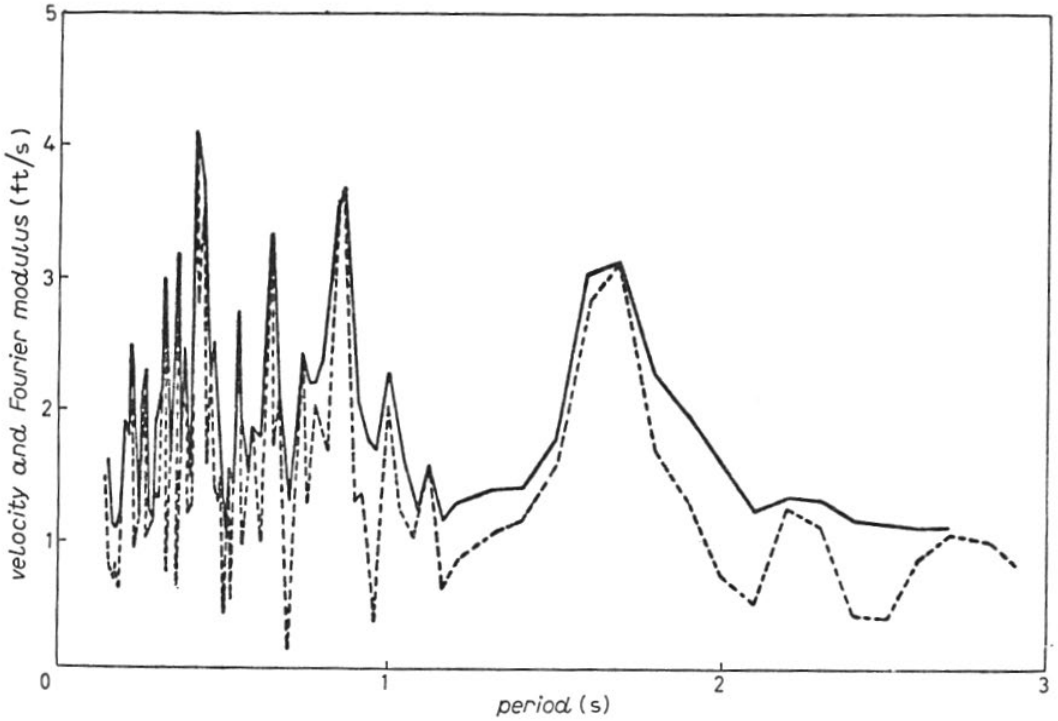

Figure 6.30. Comparison between 0%-damped response spectrum (solid line) and the Fourier amplitude spectrum (dotted line) for a strong motion record.

It is important to recognize that although the Fourier transform is a linear operator, the response spectral operator is not. That is because response spectra involves requires finding the maximum amplitude; there is no phase (timing) information in response spectra. Recall that linear operators have the property that they can be performed in any order. This is not the case for response spectra.

Response spectra were first introduced in the 1930's by Romeo Martel, who was a Caltech Professor of Mechanical Engineering. The application of response spectra was expanded by George Housner who was a Caltech Professor of Civil Engineering; Housner has been referred to as the "father of response spectral analysis."

The development of response spectral analysis preceded the development of digital computers and the calculation of spectra like that shown in Fig. 6.29 required many hours of human effort. Accordingly, researchers employed approximations that decreased numerical calculations. For example, when calculating $\max_t(x)$, the velocity $\dot{x} \approx 0$ when x is a maximum. Substituting into (6.34) gives

$$x_{\max} \approx \frac{(\ddot{u}+\ddot{x})_{\max}}{\omega_0^2} \tag{6.41}$$

This means that $S_a \approx \omega_0^2 S_d$. Also notice that when $\dot{x}$ is a maximum, then $x \approx 0$, so

$$\dot{x}_{\max} \approx \frac{(\ddot{u}+\ddot{x})_{\max}}{2\beta} = \frac{(\ddot{u}+\ddot{x})_{\max}}{2\varsigma\omega_0} \tag{6.42}$$

which means that $S_a \approx 2\varsigma\omega_0 S_v$. These approximations mean that you only need to calculate one of these response spectra (typically S_v) and then the other spectra can be approximated by simple multiplication or division with ω_0. In the 1960's it was common to determine response spectra using these simple approximations. In this case, the approximated spectra are called **pseudo response spectra**. For example, $PS_d \equiv {2\varsigma}/{\omega_0}\, S_v$ and $PS_a \equiv 2\varsigma\omega_0 S_v$. Figure 6.31 shows how these approximations can be used display all three response spectra on a single plot which is called a tripartite diagram.. It starts with a log-log plot of S_v. Diagonal logarithmic axes are added so that PS_a and PS_d can be read off of the S_v curve. This is a very clever way to show lots of information. Unfortunately, it is rarely used these days. It is most common to see S_a since it measures the maximum base shear force (mS_a).

Response spectral analysis is the language of modern earthquake engineering. It is useful to determine the excitation of the modal vibrations of buildings and it is used extensively in structural design. It's important to remember that although this theory works exceedingly well for buildings that have linearly elastic force-deformation, it must be modified to provide realistic answers for buildings that experience damage. Before I deal with the issue of inelastic, nonlinear behavior, I will introduce the theory of normal modes, which is a crowning achievement of applied mathematics. Furthermore, response spectra play a central role in this theory.

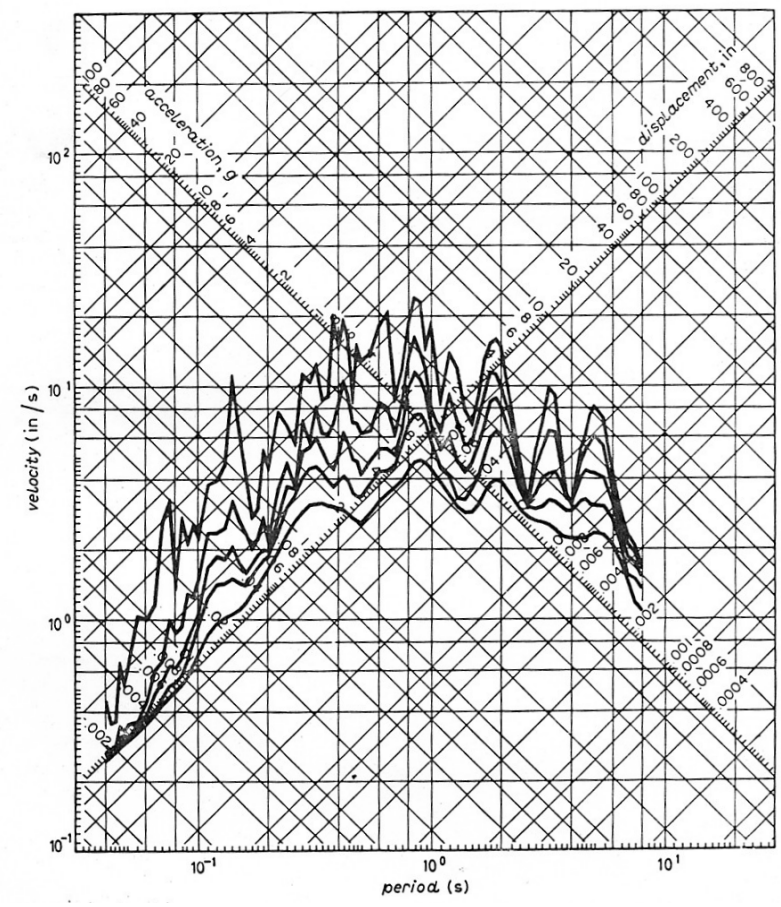

Figure 6.31. Tripartite diagram showing S_v, PS_a, PS_v for a single strong motion record and a variety of damping.

Modal Coordinate Frame

There are several different methodologies to analyze the deformations of buildings that are subjected to earthquake shaking. The situation is analogous to different approaches for solving the forced, single-degree-of-freedom, linear oscillator problem that I discussed in Chapters 1 and 2. In particular, I showed how the system responds to harmonic forces (frequency domain) or alternatively to temporal impulses (time domain). While these two approaches provide identical solutions (provided that all parts of the solutions are included), the two approaches can provide different insights into the behavior of the system. To begin, look at the displacements that were obtained by double integration of accelerations recorded in the 19-story Factor Building (UCLA, SMRF) for a M 3.6 earthquake that happened nearby in the Santa Monica Bay (Figure 6.32). Notice that the displacements in the building are primarily harmonic in nature. This is typical of all motions in buildings that experience weak shaking that can be modeled as linearly elastic. If you look closely, you will see that the motions are harmonic in both time (dominated by 3 Hz) and space (nodes at floors 1, 8, and 14). The Factor Building is unusual in that it has continuously recording 24-bit accelerometers at every floor of the

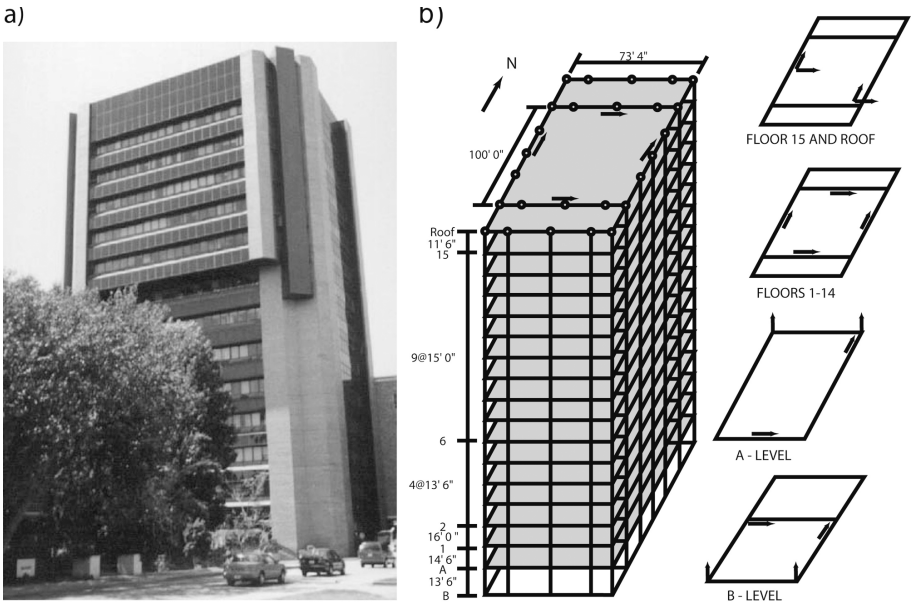

The Factor building (a) and its seismic array (b). Arrows show polarities of the single component sensor.

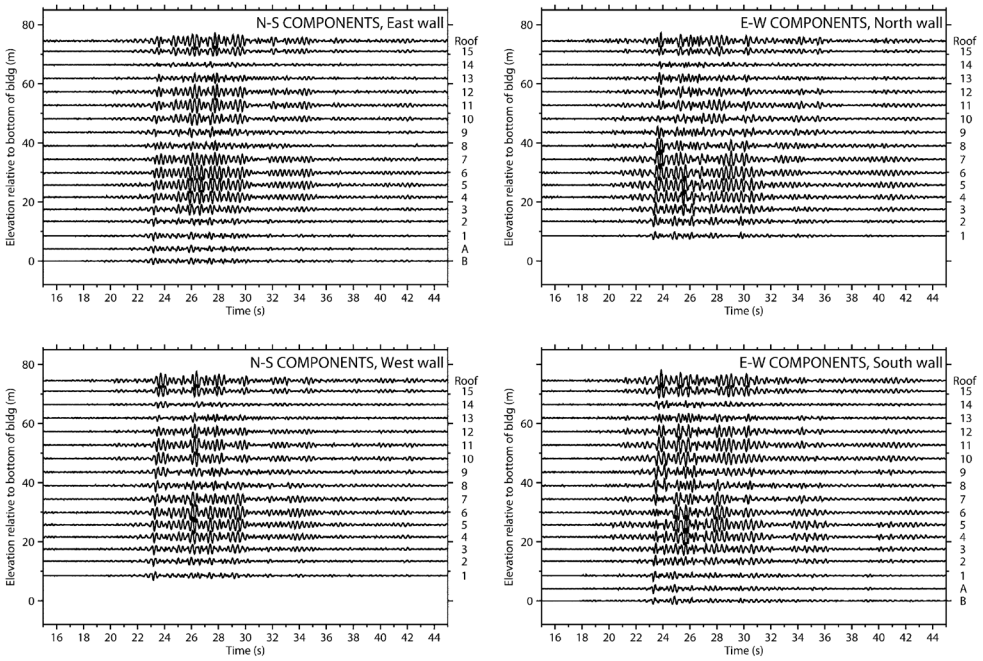

Figure 6.32 (from Kohler and others, 2007) Displacement records for the 16 December 2004 Santa Monica Bay(*M*L 3.6) earthquake. The figure shows the north–south components for sensors on the east and west walls (left), and east–west components for sensors on the north and south walls (right) except for the subbasement sensor which is on the west wall. 1 for location of sensors. Vertical numbering on the right indicates floor number with "A" for basement and "B" for subbasement.

building. The Fourier amplitude spectra of the one-day recordings of ambient vibrations recorded on each floor is shown in Figure 6.33 (from Kohler, M. D., T. Heaton, and C. Bradford, Propagating waves recorded in the steel, moment-frame Factor building during

earthquakes, Bull. Seis. Soc. Am., 97, 1334-1345, 2007). Notice that the noise at the roof level is largest in amplitude at 0.6, 1.8, and 3.0 Hz. These are the first three modes of the building. That is, the building resonates at these frequencies. Furthermore, the amplitude response of the spectral peaks is reminiscent of the amplitude response of an under-damped linear oscillator (see Chapter 1). Just as the width of the resonant peak

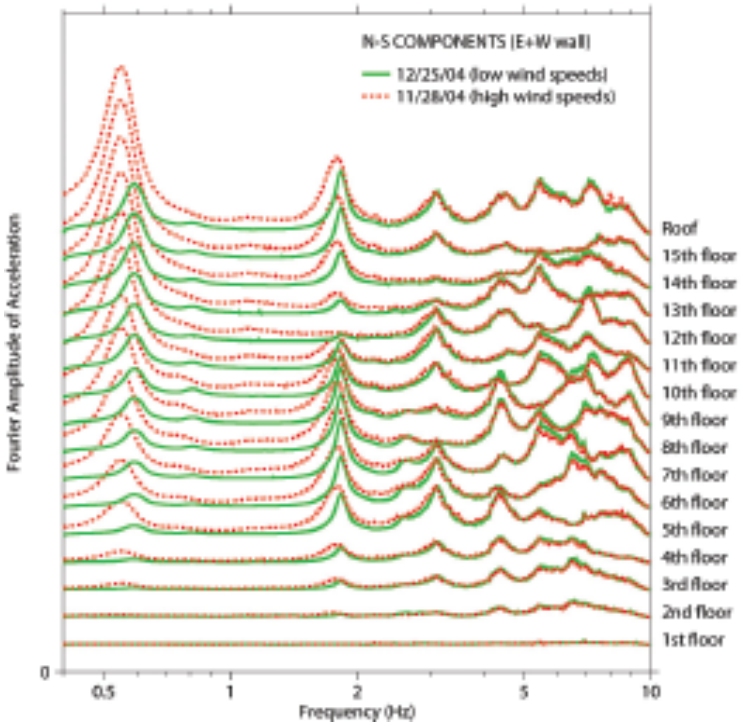

Figure 6.33. Fourier amplitude spectra of 24 hours of ambient vibrations recorded at each floor of the UCLA Factor Building.

of an sdof can be used to measure its Q (or more commonly, its fraction of critical damping), the width of the spectral peaks can be used to measure the damping of each mode of the building.

Figure 6.34 shows the amplitude of the spectral peaks as a function of the floor on which it was recorded. Notice that the first mode's amplitude as a function of height $A_1(z)$ is approximately ¼ of a wavelength of a sinusoid with a total wavelength that is four times the building's height h. That is

$$A_1(z) \approx \sin 2\pi \frac{z}{4h} \tag{6.43}$$

Furthermore, this can be generalized to the higher modes $A_n(z)$,

$$A_n(z) \approx \sin 2\pi \frac{(2n-1)z}{4h} \tag{6.44}$$

where the resonant frequency ω_n of an overtone is related to the of the frequency of the first (aka, fundamental) mode by

$$\omega_n \approx (2n-1)\omega_1 \tag{6.45}$$

These relationships are exact for the modes of a uniform beam that experiences pure shear. While they are useful for quick estimates of actual buildings, real buildings are neither uniform, nor do they experience pure shear; there is always some degree of overall bending.

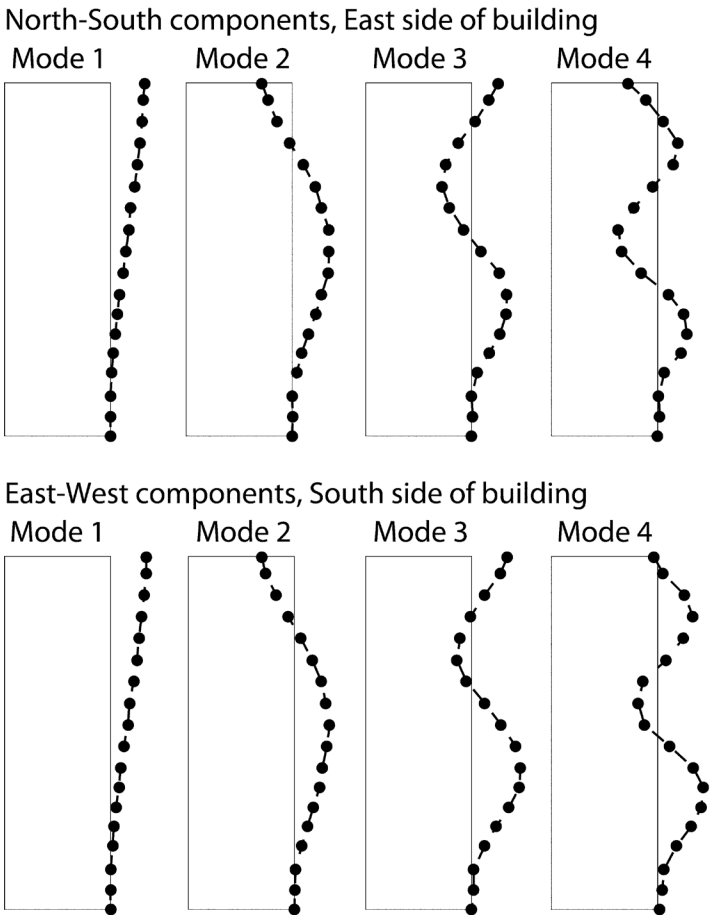

Figure 6.34. Mode shapes determined from narrowband filtered displacements recorded from the 16 December 2004 Santa Monica Bay earthquake. Filled circles represent actual sensor locations along the height of the building that contributed to the modeshape measurements.

We can gain insight into the response of a simple two-story mrf by using the simple model shown in Figure 6-35. I will assume that the horizontal motion of the base is $u(t)$ and that the first floor and the roof are rigid bodies of mass m. I will assume that the motions of the 2nd floor and the roof with respect to the base of the building is given by $x_1(t)$ and $x_2(t)$, respectively. Now assume that the columns have negligible mass and that when the 2nd floor moves relative to the base, then the columns flex and then create a

horizontal restoring force of kx_1. Similarly, assume that when the roof moves relative to the second floor, then there is a restoring force of $k(x_2 - x_1)$. I can now use Newton's 2nd law to write the equations of motion as

$$\begin{aligned} m(\ddot{x}_1 + \ddot{u}) &= -kx_1 + k(x_2 - x_1) \\ m(\ddot{x}_2 + \ddot{u}) &= -k(x_2 - x_1) \end{aligned} \tag{6.46}$$

Which can be rewritten

$$\begin{aligned} m\ddot{x}_1 + 2kx_1 - kx_2 &= -m\ddot{u} \\ m\ddot{x}_2 + kx_2 - kx_1 &= -m\ddot{u} \end{aligned} \tag{6.47}$$

This gives us two 2nd order coupled linear differential equations together with forcing terms $-m\ddot{u}$ and $-m\ddot{u}$. Just as was the case for a linear sdof, we find that the solution is comprised of the solution to the homogeneous equations plus the particular solution for the forcing terms. The homogeneous equations are

$$\begin{aligned} m\ddot{x}_1 + 2kx_1 - kx_2 &= 0 \\ m\ddot{x}_2 + kx_2 - kx_1 &= 0 \end{aligned} \tag{6.48}$$

It is convenient to rewrite (6.48) as a 2-vector equation as follows.

$$\mathbf{M}\ddot{\mathbf{x}} + \mathbf{K}\mathbf{x} = \mathbf{0} \tag{6.49}$$

where $\mathbf{x} \equiv (x_1, x_2)$, and

$$\mathbf{M} \equiv \begin{bmatrix} m & 0 \\ 0 & m \end{bmatrix} \quad \mathbf{K} \equiv \begin{bmatrix} 2k & -k \\ -k & k \end{bmatrix} \tag{6.50}$$

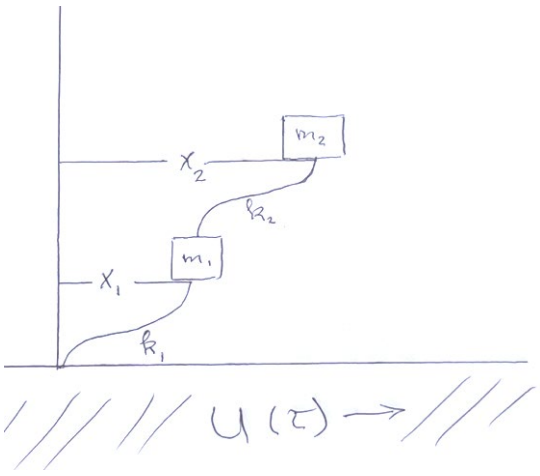

Figure 6.35 Simple model of a two-story building with lateral springs providing the restoring force of the concrete floors.

I can now guess that there are harmonic solutions. That is, assume that there is a solution in which both masses are oscillating with frequency ω, or assume that

$$\mathbf{x} = \mathbf{a}e^{i\omega t} \tag{6.51}$$

where $\mathbf{a} \equiv (a_1, a_2)$ is a 2-vector that describes the amplitude. Differentiating (6.51) twice with respect to time gives

$$\ddot{\mathbf{x}} = -\omega^2 \mathbf{a} e^{i\omega t} \tag{6.52}$$

Inserting (6.51) and (6.52) into (6.49) gives

$$-\omega^2 e^{i\omega t}\mathbf{M}\mathbf{a} + e^{i\omega t}\mathbf{K}\mathbf{a} = \mathbf{0} \tag{6.53}$$

This simplifies to

$$\left(-\omega^2 \mathbf{M} + \mathbf{K}\right)\mathbf{a} = \mathbf{0} \tag{6.54}$$

We now have two coupled linear equations with two unknowns. This is an eigenvalue problem that can be studied in most texts on linear algebra. (6.54) has nontrivial solutions if and only if

$$\det\left(-\omega^2 \mathbf{M} + \mathbf{K}\right) = 0 \tag{6.55}$$

This equation is known as the **characteristic equation** which can be used to find the resonant frequencies. Inserting (6.52) into (6.55) gives

$$\det\begin{bmatrix} 2k - \omega^2 m & -k \\ -k & k - \omega^2 m \end{bmatrix} = \omega^4 m^2 - 3k\omega^2 m + k^2 = 0 \tag{6.56}$$

The quadratic formula can be used to solve (6.56) for ω^2. This gives

$$\omega^2 = \left(\frac{3 \pm \sqrt{5}}{2}\right)\frac{k}{m} \tag{6.57}$$

The fundamental mode is the lowest frequency solution and it is

$$\omega_1 = \sqrt{\frac{3-\sqrt{5}}{2}}\sqrt{\frac{k}{m}} = 0.618\omega_0 \tag{6.58}$$

The 2nd frequency, the overtone frequency is

$$\omega_2 = \sqrt{\frac{3+\sqrt{5}}{2}}\sqrt{\frac{k}{m}} = 1.628\omega_0 \tag{6.59}$$

where $\omega_0 \equiv \sqrt{k/m}$, which is the frequency of a simple sdof using the same spring and mass. (6.58) can be inserted into (6.54) to solve for $\mathbf{a}_1$, which tells us the relative motion of the two masses when they are in free vibration (homogeneous solution) at ω_1. That is,

$$\left(-\omega_1^2 \mathbf{M} + \mathbf{K}\right)\mathbf{a}_1 = \mathbf{0} \tag{6.60}$$

or

$$\begin{bmatrix} 2k - \omega_1^2 m & -k \\ -k & k - \omega_1^2 m \end{bmatrix}\begin{bmatrix} a_{11}, a_{12} \end{bmatrix} = \begin{bmatrix} 0 \\ 0 \end{bmatrix} \tag{6.61}$$

substituting (6.58) into (6.61) gives

$$\begin{bmatrix} 2k - \dfrac{3-\sqrt{5}}{2}k & -k \\ -k & k - \dfrac{3-\sqrt{5}}{2}k \end{bmatrix}\begin{bmatrix} a_{11}, a_{12} \end{bmatrix} = \begin{bmatrix} 0 \\ 0 \end{bmatrix} \tag{6.62}$$

So

$$\left(\frac{1+\sqrt{5}}{2}\right)a_{11} = a_{12} \qquad a_{11} = 0.618a_{12} \tag{6.63}$$

Which means that, when the system is resonating at the first mode, the amplitude of the top floor is 1.6 times larger than the 2nd floor; the amplitude of the base is, by definition zero. Since $\mathbf{a}_1$ is real, there are no phase lags between the floors and the floors move completely in phase.

The second mode can be found in a similar way. Inserting (6.59) into (6.54) gives

$$\begin{bmatrix} 2k - \dfrac{3+\sqrt{5}}{2}k & -k \\ -k & k - \dfrac{3+\sqrt{5}}{2}k \end{bmatrix} \begin{bmatrix} a_{21}, a_{22} \end{bmatrix} = \begin{bmatrix} 0 \\ 0 \end{bmatrix} \tag{6.64}$$

or

$$\frac{1-\sqrt{5}}{2}a_{21} = a_{22} \qquad -0.618a_{21} = a_{22} \tag{6.65}$$

Which means that the 2nd floor moves opposite to the roof. Notice that

$$\mathbf{a}_1 \bullet \mathbf{a}_2 = a_{11}a_{21} + a_{12}a_{22} = 0 \tag{6.66}$$

Which tells us that the amplitude vectors (the eigenvectors) are orthogonal. This is a general property that is true as long as the system is purely elastic. I can now write the general solution to (6.49)

$$\mathbf{x}(t) = a_1 \begin{bmatrix} 1 \\ 1.618 \end{bmatrix} \cos(\omega_1 t - \delta_1) + a_2 \begin{bmatrix} -0.618 \\ 1 \end{bmatrix} \cos(\omega_2 t - \delta_2) \tag{6.67}$$

where $a_1, a_2, \delta_1, \delta_2$ are four constants that allow the solution to fit the initial conditions (velocity and displacement for each mass). Notice that I can define a new coordinate system (ξ_1, ξ_2) where

$$\begin{aligned} \xi_1 &\equiv 0.851(0.618x_1 + x_2) \\ \xi_2 &\equiv 0.851(0.618x_1 - x_2) \end{aligned} \tag{6.68}$$

ξ is called the modal coordinate frame and it decouples two coupled ode's for (x_1, x_2) into two uncoupled ode's. These coordinates have been normalized to have unit length and they are are orthogonal, which means that they are basis vectors. Using this new modal coordinate frame results in two equations that are a linear sdof that is extensively discussed in Chapter 1.

Of course, a model of a building that consists of two identical floors is of limited practical value. However, the approach to the problem can be generalized to cover any system of n point masses that are connected by linearly elastic springs and linear viscous dampers. In this case, the problem is written as

$$\mathbf{M}\ddot{\mathbf{x}} + \mathbf{C}\dot{\mathbf{x}} + \mathbf{K}\mathbf{x} = -\mathbf{M}\ddot{u} \tag{6.69}$$

Where $\mathbf{x}$ is a Cartesian n-vector that describes the motion of the discrete masses, $\mathbf{M}$ is the $n \times n$ mass matrix, $\mathbf{C}$ is the $n \times n$ damping matrix, and $\mathbf{K}$ is the $n \times n$ stiffness matrix. In many cases, the mass and stiffness matrices can be constructed using induction from simpler problems. However, sometimes these matrices are not obvious. In these instances, it is best to use a Lagrangian (kinetic energy minus the potential energy) to derive these matrices.

Once the building is described as an n-degree-of-freedom linear system (i.e., (6.69)), then there are several methods to solve the eigen-value problem for the homogeneous solution. Since the damping forces are not known *a priori*, it is best to begin with the approximation that $\mathbf{C} \approx \mathbf{0}$. The eigenvalues $\left(\omega_1, ..., \omega_n\right)$ are then computed. Since there is no damping, these eigenvalues are all real valued, which means that all of the masses vibrate in phase (except for possible π phase shifts). Once the n eigenvalues (modal frequencies) are found, then the n corresponding eigenvectors (the mode shapes) can be determined. These eigen vectors are then normalized to have a length of 1. The set of eigenvectors are all orthogonal to each other and the normalized eigen vectors can be used as a set of basis vectors $\left(\mathbf{a}_1, ..., \mathbf{a}_n\right)$ to describe any solution to the problem. At that point, the problem is then transformed into

$$\mathbf{x}_i\left(t\right) = \mathrm{Re}\left(\mathbf{a}_i e^{i\omega_i t}\right) \tag{6.70}$$

where $\mathbf{a}_i$ is an $n \times 1$ vector that satisfies

$$\left(\mathbf{K} - \omega_i^2 \mathbf{M}\right)\mathbf{a}_i = \mathbf{0} \tag{6.71}$$

There is always a rotation matrix , $\mathbf{Q}$, that will transform $\mathbf{K} - \omega_i^2 \mathbf{M}$ into a diagonal matrix

$$\mathbf{Q}\left(\mathbf{K} - \omega_i^2 \mathbf{M}\right)\mathbf{Q}^T \mathbf{a}_i = \begin{bmatrix} \xi_1 & & & \\ & \cdot & & \\ & & \cdot & \\ & & & \xi_n \end{bmatrix} \tag{6.72}$$

If this equation is rotated into the modal coordinate system, then the n coupled equations transforms into n decoupled equations.

While the mass and stiffness can be derived from the dimensions of the structural elements, the damping is far more problematic. If a building is driven by an impulse to its free vibrations, then the building would oscillate forever if there was no damping. Obviously, there is damping in real buildings. The simplest way to estimate building damping is using the modal coordinate frame. In particular, the width of the modal resonant peaks gives an estimate of the damping for the mode. This is fairly straightforward for the fundamental modes whose resonant frequencies are well separated from the higher modes. Unfortunately, it can be tricky to identify the characteristics of the resonant peaks of higher modes since these frequencies may be closely spaced.

The use of normal modes to simulate building vibrations assumes that damping can be described as linear viscous. That is, we assume that there is a damping matrix $\mathbf{C}$. The

introduction of this damping matrix complicates the eigenvalue problem. While it's still a problem in linear algebra, the eigenvalues (resonant frequencies) are now complex numbers, which means that motions decay exponentially in time. Unfortunately, the eigenvectors also have complex amplitudes, which means that there are phase lags between the masses that oscillate at an eigenfrequency. However, if $\mathbf{C} = c_1\mathbf{M} + c_2\mathbf{K}$, then the eigenvectors are real-valued even though the eigenvalues are complex. The assumption that the damping matrix can be written as a linear sum of the mass and stiffness matrices is common and its referred to as **Rayleigh damping**.

Although damping is an important issue, it is rarely measured. In particular, the small-amplitude damping of the fundamental modes of tall buildings is probably about 1% to 2%. However, it is standard that 5% damping is assumed for almost all design calculations. The general idea is that damping increases with the amplitude of the excitation, and that 5% is a reasonable approximation of reality. I will shortly show that 5% is a gross underestimate for a building that undergoes significant damage. Unfortunately, this endemic error has profound implications for the design of buildings. I will cover this issue when I discuss the behavior of inelastic, nonlinear systems. Before I get to that problem, I want to discuss another method to analyze elastic linear buildings. This technique is based on propagating waves and it's more familiar to seismologists.

Flexible Building as a Continuous Cantilevered Beam

The problem of the dynamic motions of a continuous prismatic beam can give us some insight into the deformation of buildings. To solve such a cantilevered beam problem in full generality is exceedingly complex. To begin with we recognize that, if the building is considered as a continuum, it would often be anisotropic. For example, consider a moment-resisting frame (e.g., Fig. 6.5). Assume that the 1 and 2 axes are horizontal and that the 3 axis is vertical, The building stiffness associated with inter-story drift $(\varepsilon_{13}$ and $\varepsilon_{23})$ would be much less than the stiffness associated with in-plane shearing of the actual floor slabs ε_{12}. Likewise the stiffness associated with extension along columns (ε_{33}) is different than for extension along the floor slabs $(\varepsilon_{11}$ and $\varepsilon_{22})$. However, we will assume that only the parts of the strain tensor that are important to describe the deformation of the building are the inter-story shear strain and the extensional strain along the columns. We can thus approximate the building as being isotropic, since the other elastic moduli are not important. We must also recognize that the material in our imaginary continuous beam may have a very unusual Poisson's ratio. That is, the building is very stiff in compression along the columns and very flexible in inter-story shear. That is, $E \gg \mu$. In fact, for a tall mrf (either concrete or steel), the velocity of longitudinal-waves up the building $\left(\sqrt{E/\rho_{eff}}\right)$ is 10 to 20 times more than the inter-story S-wave velocity $\left(\sqrt{\mu_{eff}/\rho_{eff}}\right)$.

While the complete solution for an isotropic elastic cantilevered beam is itself quite complex, there are two end-member cases where the solution is more tractable (see figure 6.36).

The first is the case in which the height of the building is large compared to the length of the base (a tall skinny building). In this case the building deforms primarily by bending, which is the term used for extensional strains in the columns (extension and compression in the columns at the opposite sides of the building). There is a well-developed theory that allows beam problems to be solved with the assumption that the shear strains are approximately zero (the technical theory of bending). This is called a **bending beam**. The stiffness of a bending beam is determined by its flexural rigidity, *EI*, which scales with dimension as

$$EI = E\int_0^w\int_0^w x_1^2 dx_1 dx_2 = \frac{E}{3}w^4 \tag{6.73}$$

where *E* is the Young's modulus and the building is assumed to have a square cross section of width *w*. The building becomes very stiff against flexure as *w* becomes large. It's easier to bend a thin rod than it is a pipe having the same total mass per unit length.

In the second case the building is assumed to be much wider than it is tall. When the ground beneath the building moves horizontally, this is identical to the problem of having an SH wave propagate vertically in a layer of building; the bending is approximately zero in this case. This is called a **shear beam.** In this case the total stiffness against shear is just the shear modulus times the cross sectional area $\left(\mu w^2\right)$. Therefore, it is easy to see why a wide building is dominated by shear and not by bending.

While actual buildings are neither a true bending beam nor a shear beam, we can gain some useful insight by looking at these approximate modes of deformation.

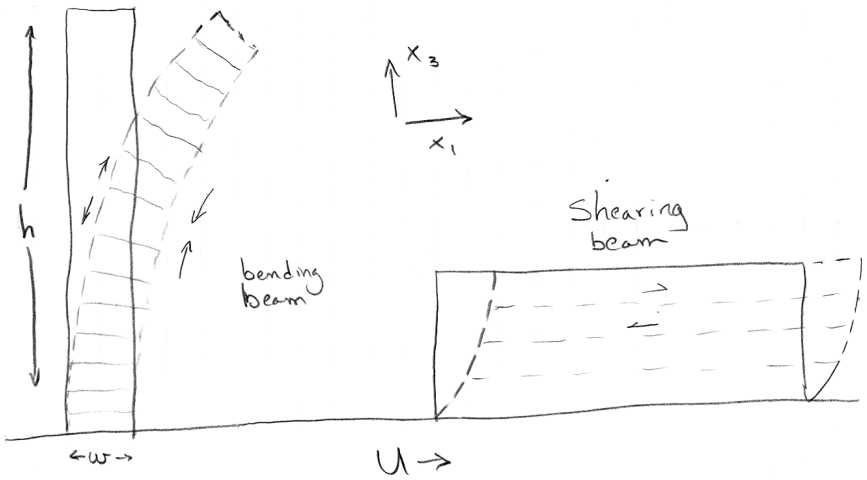

Figure 6.36. Cartoon on the left is a bending beam (negligible inter-story shear strains). Most of the deformation occurs because of compression and extension of the outer

columns. Cartoon on the right is a shearing beam (negligible extension/compression on the columns). The floor slabs remain horizontal.

Flexible Building as a Shearing Beam

Figure 6.37 shows the horizontal accelerations that occurred on different floors of a 52-story steel mrf building in downtown Los Angeles during the 1994 Northridge earthquake. Notice the prominent pulse of acceleration that occurs at the base of the building at about 14 seconds into the record. This pulse can be observed to propagate up the building and it arrives at the top about 1.5 seconds later. Also notice that the pulse is twice as large on the roof as it is in the rest of the building. You can even see a hint that the pulse travels back down the building after it reflects off the top. This type of behavior is exactly what we expect from a shear beam. It is identical to the problem of a vertically propagating SH wave in a plate with a rigid boundary at the bottom and a free boundary at the top. I already extensively discussed this problem in Chapter 4.

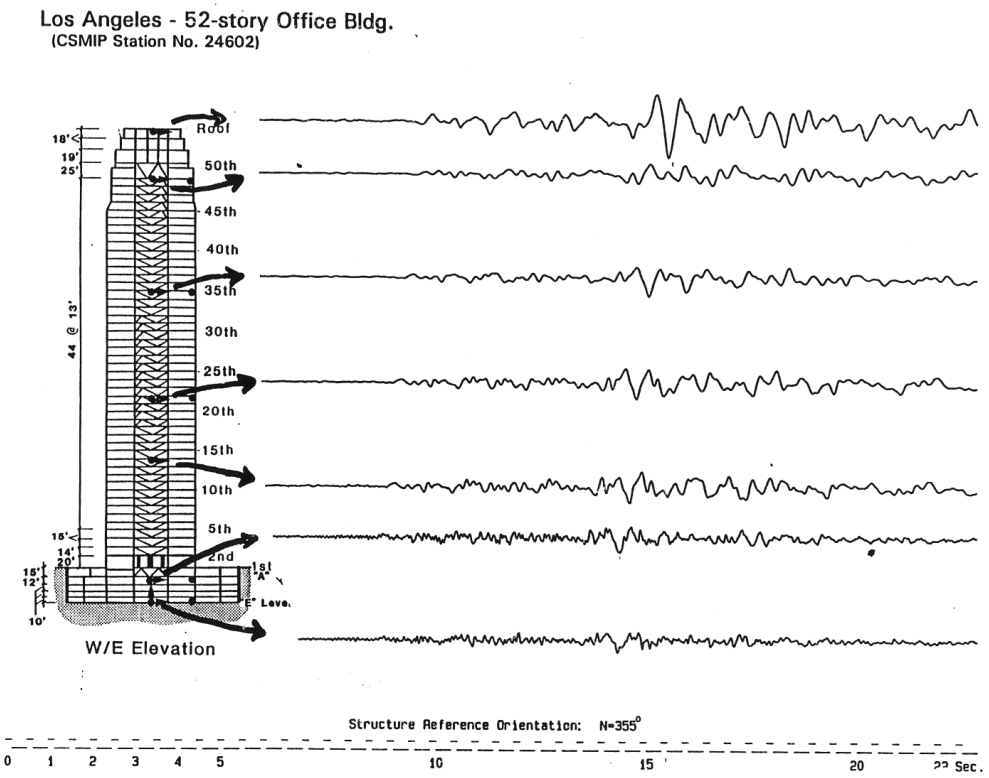

Figure 6.37. Horizontal accelerations in a steel mrf during the 1994 Northridge earthquake. Notice the vertically propagating pulse.

Figure 6.38 shows four other examples of SH-waves propagating vertically in a steel-frame building. The motions recorded at the ground level have been deconvolved from

all of the records to show the response of the building to an impulse of horizontal displacement at the base.

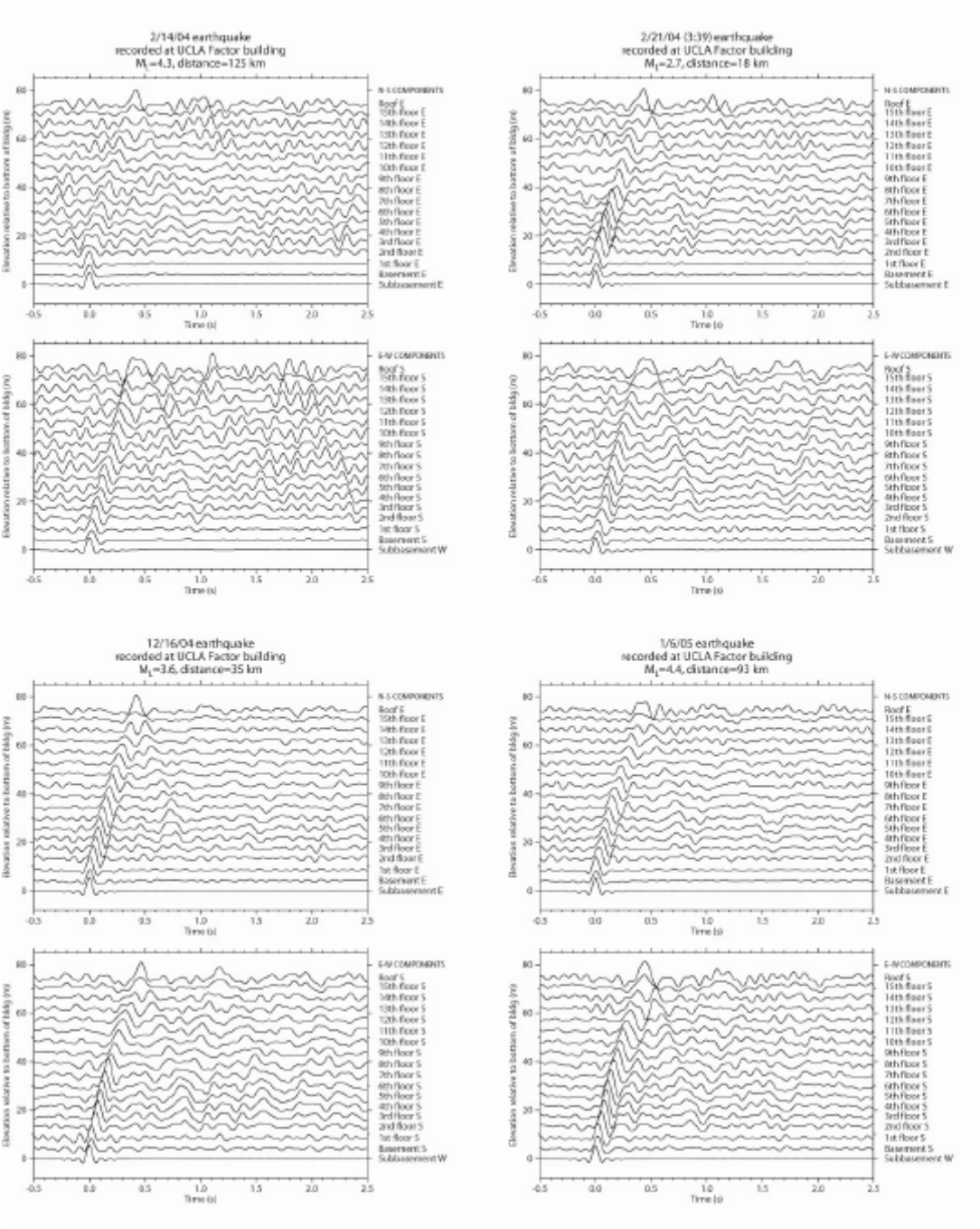

Figure 6.38. Individual impulse response functions for four earthquakes recorded in the UCLA Factor Building. (a) 14 February 2004, (b) 21 February 2004 (3:39 UTC time), (c) 16 December 2004, and (d) 6 January 2005. See Table 1 for more information about these earthquakes. Each earthquake's pair of plots shows the north–south components for sensors on the east wall (top) and east–west components for sensors on the south wall, except for the subbasement sensor which is on the west wall. For clarity, we show only those walls that had a subbasement sensor.

In chapter 4, we saw that the solution to this problem can be written as a sum of reflecting SH-wave pulses. The motion in the building is given by

$$u_1(t,x_3)=u_1^g\left(t-\frac{x_3}{c}\right)+u_1^g\left(t-\frac{2h}{c}+\frac{x_3}{c}\right)-u_1^g\left(t-\frac{2h}{c}-\frac{x_3}{c}\right)$$
$$-u_1^g\left(t-\frac{4h}{c}+\frac{x_3}{c}\right)+u_1^g\left(t-\frac{4h}{c}-\frac{x_3}{c}\right)+.... \tag{6.74}$$

where c is the shear-wave velocity in the building and $u_1^g(t)$ is the horizontal motion of the ground at the base of the building. Notice that this sequence repeats with periodicity $\frac{4h}{c}$, which is the fundamental period of the building oscillation. We are particularly interested in the drift in the building ε_{13}, which we can calculate from (6.74).

$$\varepsilon_{13}(t,x_3)=\frac{1}{c}\left[-\dot{u}_1^g\left(t-\frac{x_3}{c}\right)+\dot{u}_1^g\left(t-\frac{2h}{c}+\frac{x_3}{c}\right)+\dot{u}_1^g\left(t-\frac{2h}{c}-\frac{x_3}{c}\right)\right.$$
$$\left.-\dot{u}_1^g\left(t-\frac{4h}{c}+\frac{x_3}{c}\right)-\dot{u}_1^g\left(t-\frac{4h}{c}-\frac{x_3}{c}\right)+....\right] \tag{6.75}$$

We are especially interested in the drift at the base of the building $(x_3=0)$, or

$$\varepsilon_{13}^b(t)=\frac{1}{c}\left[-\dot{u}_1^g(t)+2\dot{u}_1^g\left(t-\frac{2h}{c}\right)-2\dot{u}_1^g\left(t-\frac{4h}{c}\right)+....\right] \tag{6.76}$$

That is at the base of the building, the up- and down-going waves interfere destructively to give zero displacement (remember it's a rigid base), but the associated strains interfere constructively to give twice as large a drift. Notice that the drift at the top of the building is zero, even though the motion is twice as large as in the rest of the building.

The actual drift in the base of our shear beam depends on the nature of the ground velocity $\dot{u}_1(t)$. Although strong shaking in earthquakes can take a wide variety of forms, it is common that ground displacements near large ruptures have motions described by a pulse of displacement (sometimes referred to as the "killer pulse"), or in other cases they may be dominated by the permanent offset of the ground with respect to an inertial reference frame. Consider the simple ground motions shown in Figure 6.22. The ground accelerations consist of a sequence of positive and negative constant steps. This results in ground velocity that consists of a number of linear ramps. The solution to this problem is simple as long as the duration of the pulse is shorter than the time required for the wave to travel up the building and then return $\left(\frac{2h}{c}\right)$. Things get more complex when the duration of the ground motion becomes large. Of interest is the maximum shear strain at the base of the building, which we can write as

$$\left|\varepsilon_{13}^b\right|_{\max}=\frac{\left|\dot{u}_g\right|_{\max}}{c}A \tag{6.77}$$

where A is an amplification factor. For ground motions A and B, A depends on T_p/T_1, where $T_1=4h/c$ is the fundamental period of the building. The factor A reaches 2 for

ground motion A (when $T_p \le T_1$) and 4 for ground motion B (when $T_p = T_1$). Plots of $\varepsilon_{13}^b(t)$ for $T_p = T_1$ are shown in Figure 6.39. The configurations of the building at different times are shown in Figure 6.40.

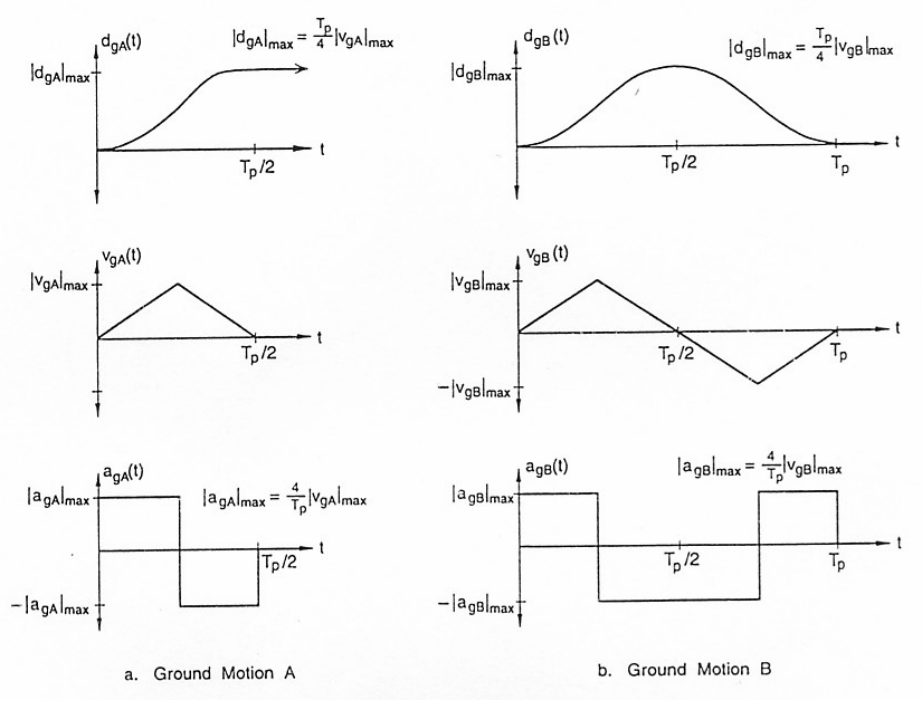

Figure 6.39. Simple ground motions that consist of a simple static displacement (case A) and a pulse of displacement (case B).

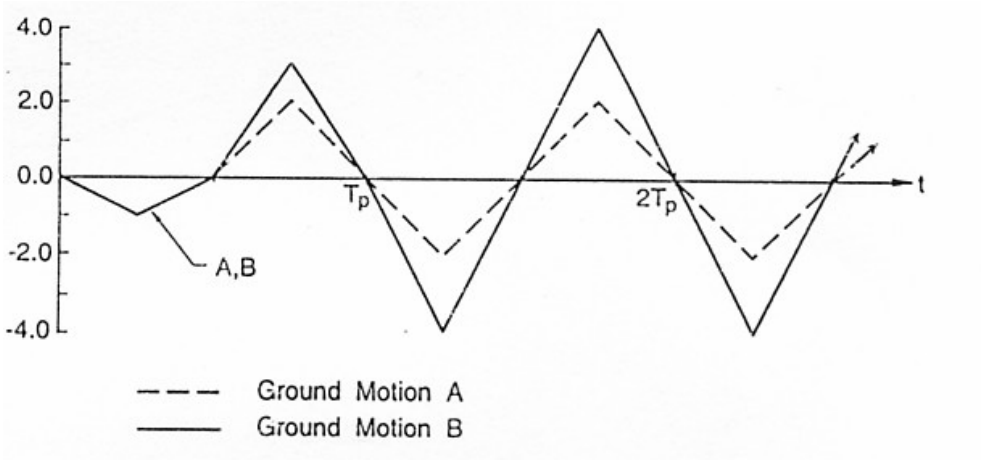

Figure 6.40. Shear strain in the base of the building. One unit on the vertical axis corresponds to a strain of $\dfrac{c\varepsilon_{13}^b(t)}{|\dot{u}_g|_{max}}$.

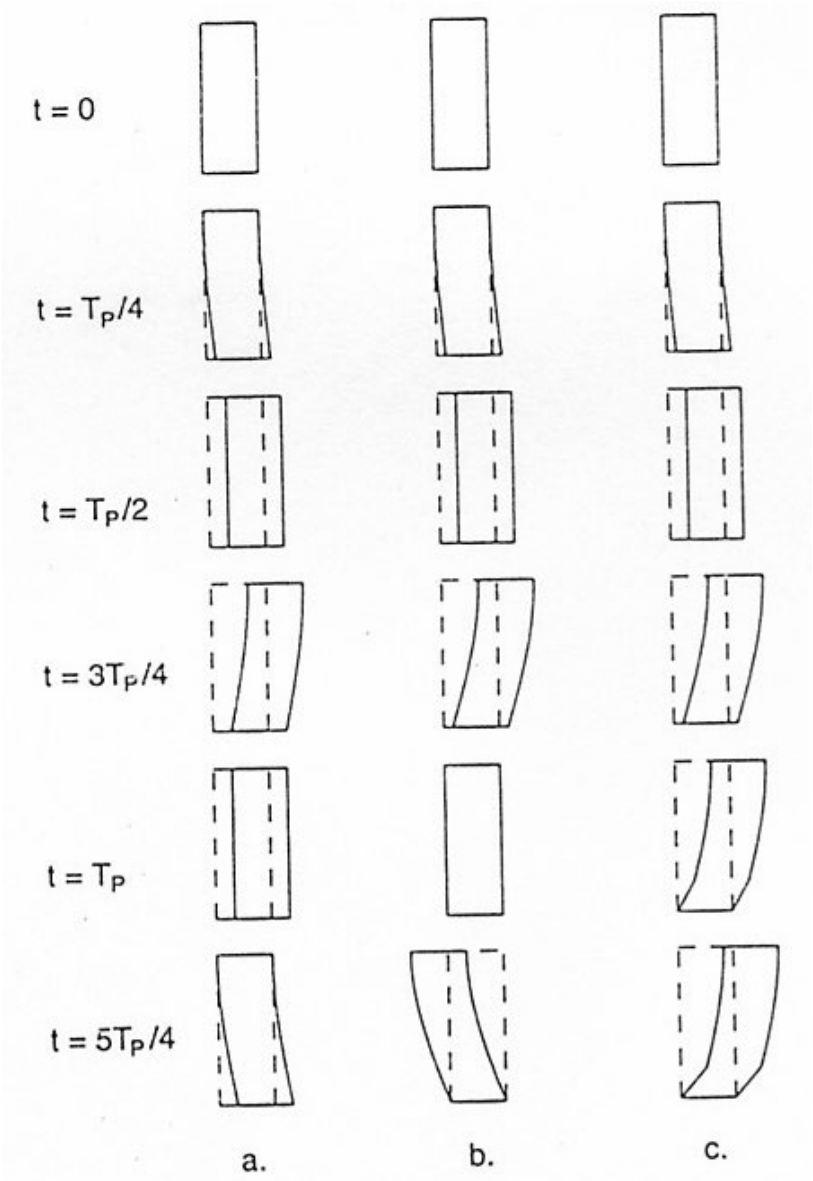

Figure 6.41. Configuration of a multi-story building at time intervals of $T_p/4$ for the case $T_p = T_1$. a) Elastic shear beam building for ground motion A. b) Elastic shear beam building for ground motion B. c) Inelastic shear beam building for ground motion B (qualitative depiction).

The shear strain $\left|\varepsilon_{13}^{b}\right|_{\max}$ can be large enough to be well into the inelastic range. With $\left|\dot{u}_g\right|_{\max} = 1\,\text{m/s}$, and $c = 100\,\text{m/s}$ (a typical value for a tall building), we can use (6.77) and Figure 6.39 to calculate that $\left|\varepsilon_{13}^{b}\right|_{\max} = 0.02$ for ground motion A and 0.04 for ground motion B, when $T_p = T_1$. These are large values and can greatly exceed the yield strain at the base of the building (e.g., check out Figure 6.10).

The dynamics problem becomes far more complex when the building experiences yielding. That is the governing equations are no longer linear and it is generally necessary to perform a careful finite-element analysis to understand the deformation of the structure. Such an analysis was performed by Hall and others (1995), and the typical results are shown in Figure 6.41. Figure 6.42 shows the location of weld failures (moment resisting connections) in the structure.

When the building yields, it tends to develop a permanent bend in the structure. Once a tall frame building is permanently bent, there is really no practical way to straighten it again, and it is a total loss. Furthermore, if the bending exceeds several percent locally, then there may be a real fear of collapse due to P-Δ effects.

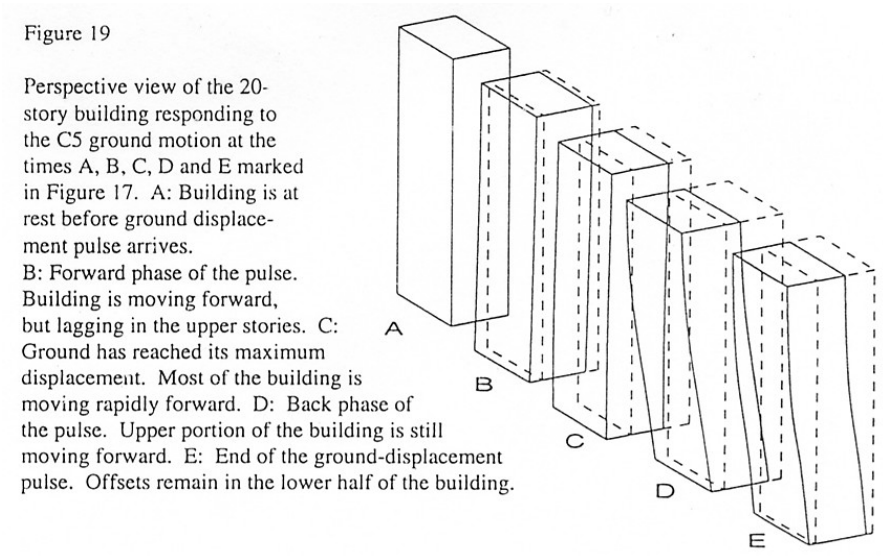

Figure 6.42 From Hall and others (1995).

One way to gain some insight into the behavior of a yielding beam is to consider the building as if it were linear, but with a local stiffness that changes with the amplitude of the local drift. For example, the slope of the force-drift curve in Figure 6.6 is called the tangent stiffness, and it rapidly decreases when the building begins to yield (it even changes sign). Since the stiffness is critical in determining the velocity at which a deformation propagates up a building, loss of stiffness due to yielding means that deformations tend to slow their propagation up a building. That is, once yielding begins, deformations tend to localize in these yielding zones. Perhaps an example of this is shown in Figure 6.44 in which an 8-story building lost the 6th story during the 1995 Kobe earthquake. That is, when ground motions are propagating in a building, then once yielding begins at a particular place, then that is where the majority of the strain will occur.

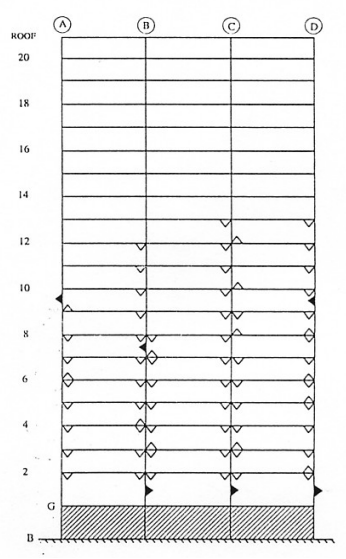

Figure 6.43. Distribution of weld fractures in a 20 story building caused by a 2 meter displacement pulse as reported by Hall and others (1995). A dark triangle locates a cracked column-flange weld at a column splice due to tension in the column. These can be very serious, since if the column separates in tension, but does not come back together properly, the column may fail to carry the weight of the building (very bad). Open triangles locate failed moment-frame connections, which causes a loss of ductility, but is not as serious as failure of a column splice.

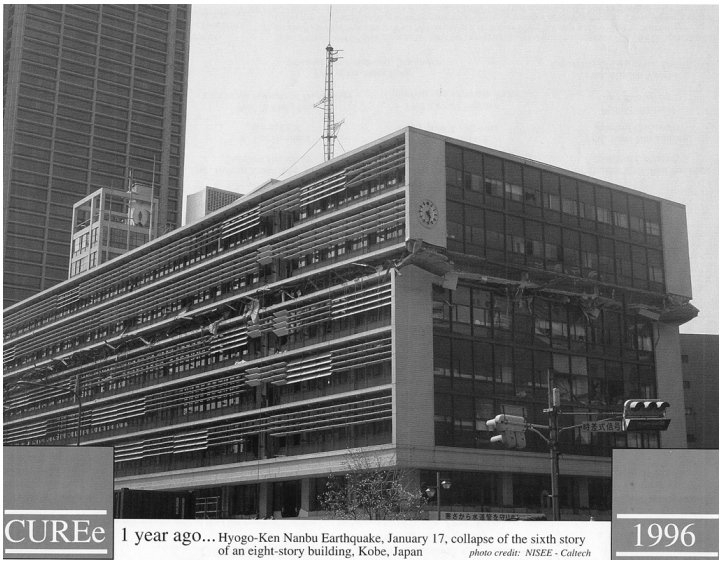

Figure 6.44. Once yielding begins at some location, then the loss of stiffness at that location can tend to localize the deformations to that location. This may have been the cause of the collapse of the 6th floor of this 8-story building in Kobe in 1995.

Prediction of the collapse of structures is extremely difficult. That is, the failure of a critical component (such as a weld) may cause loads carried by a structural element to be transferred to others structural elements, which may cause a cascade of failures. Assessing the likelihood of failure means obtaining an accurate understanding of all of

these interrelations (highly nonlinear and perhaps chaotic). Consider the three identical 21-story steel mrf towers in Mexico City that experienced the 1995 Michoacan earthquake (Figure 6.45 and 6.46). This was not a failure due to the propagation of a displacement pulse. Instead, it was due to amplification of 2-second ground motions by the shallow sediments beneath Mexico City (see Chapter 4).

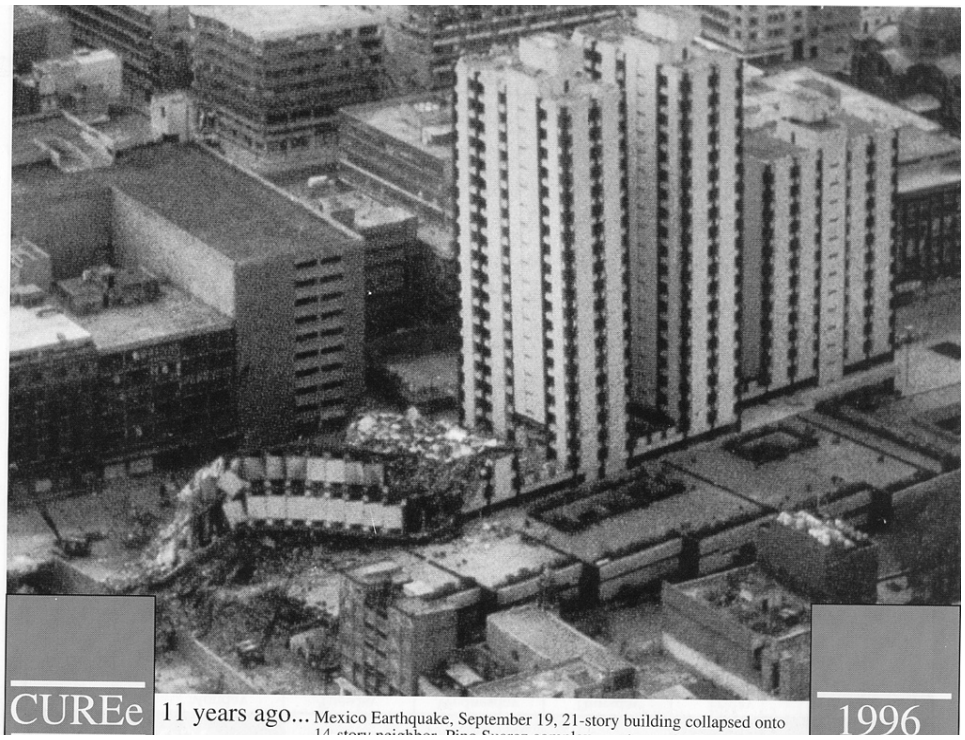

Figure 6.45. Three 21-story steel mrf's that were designed to be identical. The left tower collapsed, the middle tower had a 1-meter permanent drift of its roof, and the right tower suffered no apparent damage. (Mexico City following the 1985 Michoacan earthquake).

Figure 6.46. Close-up of the left tower in Figure 6.45.

Although the three towers were designed to be the same, their behavior was quite different, despite their close proximity to each other. The tower on the right suffered no apparent damage as a result of the shaking. The tower on the left collapsed, while the tower in the middle had a permanent roof drift of about 1 meter. It would be very difficult to explain this difference by current state of the art in numerical modeling of these buildings.

Soil-Structure Interaction for a Shear Beam

As long as we are treating the shear-beam building as if it was a low-velocity, low-density layer on the top of the Earth, we can gain some insight into how the building interacts with the soil layers. For instance, we can ask 1) how much does the presence of the building change the ground motion at its base compared to the ground motion that would have occurred without the presence of the building (a free field site), and 2) how much of the motion of the building is transmitted through the base of the building when a wave reflects off the top of the building and then transmits through the base of the building?

From Chapter 4 we know that for an SH-wave vertically incident on the base of a layer of buildings,

$$\begin{aligned}\frac{A_B^T}{A_G^I} &= \frac{2\mu_G\beta_B}{\mu_G\beta_B + \mu_B\beta_G} \\ &= \frac{2\beta_B\rho_B}{\beta_G\rho_G + \beta_B\rho_B} \approx 2\left[1 - \frac{\beta_B\rho_B}{\beta_G\rho_G} + \left(\frac{\beta_B\rho_B}{\beta_G\rho_G}\right)^2 + \ldots\right]\end{aligned} \tag{6.78}$$

where A_B^T is the amplitude of the wave transmitted into the building and A_G^I is the amplitude of the incident wave from the ground. Let us suppose that the shear wave velocity in the soil is approximately twice that in the building (a fairly soft soil), and that the density of the building is 5% of the density of the soil, then

$$\frac{A_B^T}{A_G^I} \approx 2\left(1 - 0.025\right) = 1.975 \tag{6.79}$$

But the amplitude of the motion without the building is 2.0 because it is an SH reflection off of the free surface. Therefore the building causes the amplitude of the motion to be decreased by 1 ¼ % relative to the ground motion that would have occurred without the presence of the building. This soil-structure interaction effect seems to be far less important than the effect of allowing the building to rock on its foundation (discussed earlier in this chapter).

We can also compute the size of the wave reflected off the base of the building A_B^R compared with the amplitude of the down-going wave in the building A_B^I. That is

$$\frac{A_B^R}{A_B^I} = \frac{\beta_B \mu_G - \beta_G \mu_B}{\beta_B \mu_G + \beta_G \mu_B} = \frac{\mu_G^2 \mu_B \rho_G - \mu_B^2 \mu_G \rho_B}{\mu_G^2 \mu_B \rho_G + \mu_B^2 \mu_G \rho_B + 2\mu_G \mu_B \sqrt{\mu_G \mu_B \rho_G \rho_B}} \tag{6.80}$$

If the density of the ground is large compared to the building $\left(\rho_G \gg \rho_B\right)$, then

$$\frac{A_B^R}{A_B^I} \approx \frac{\mu_G^2 \mu_B \rho_G - \mu_B^2 \mu_G \rho_B}{\mu_G^2 \mu_B \rho_G} = 1 - \frac{\rho_B \mu_B}{\rho_G \mu_G} = 1 - \left(\frac{\rho_B \beta_B}{\rho_G \beta_G}\right)^2 \tag{6.81}$$

Therefore, most of the wave is reflected off the base of the building. For the previous case, the reflected wave is 99.94% the amplitude of the incident wave.

Bending Beam

It is not possible to solve the bending beam problem in the same way that we did the shearing beam. For the technical theory of bending, the horizontal displacements of the building obey the Bernoulli-Euler equation, which is

$$EI \frac{\partial^4 u_1\left(x_3, t\right)}{\partial x_3^4} = -\rho S \frac{\partial^2 u_1\left(x_3, t\right)}{\partial t^2} \tag{6.82}$$

where S is the cross-sectional area of the building ($= w^2$ if the building has a square cross section). Whereas Navier's equation was a second order equation, the Bernoulli-Euler bending beam equation is a fourth order equation. Fortunately, this is still a linear equation. However, it is no longer true that there is a unique velocity such that $u_1 = f\left(t - x_3/c\right)$ solves this equation. We can try a traveling harmonic wave; that is assume that

$$u_1 = \sin\left(k_n x - \omega_n t\right) \tag{6.83}$$

Direct substitution indicates that (6.83) is a solution to (6.82) if

$$\frac{\omega_n}{k} = \sqrt{\omega_n} \sqrt[4]{\frac{EI}{\rho S}} \tag{6.84}$$

But ω_n / k_n is just the phase velocity c_n of this traveling harmonic wave. Therefore, we see that the phase velocity of a traveling harmonic waves increases as the square root of the frequency of the wave. Since (6.82) is linear, we can form a more general solution of the form

$$u_1 = \sum_n C_n \sin k_n \left(x - c_n t \right) \tag{6.85}$$

where the c_n's are constants. Since the different frequencies travel at different velocities, the waveform will change as the wave propagates. This is known as dispersion. There is probably some dispersion that occurred in the propagation of the pulse in the building shown in Figure 6.37. This may explain why it becomes difficult to distinguish the pulse after it has propagated a long distance in the building.

Misunderstanding of modal damping

As can be seen in Fig. 6.29, the amplitude of a response spectra varies strongly with the assumed damping. While undamped response spectra are similar to Fourier amplitude spectra, they grow ever more different with increasing damping. Remember that there is no information about the arrival of phases contained in Fourier amplitude spectra. Even if the time-domain record has the arrival of a pulse that has a broad frequency content, the spectrum of the entire record usually continues to vibrate for a long time (we call it coda). This coda is often comprised of resonances in the low-velocity materials near the Earth's surface. As the damping increases, the response spectrum becomes more sensitive to the largest transients (e.g. pulses). Attempts to measure the small amplitude damping of tall buildings indicates that 2 % is typical (reference). However, it is widely believed that inelastic dissipation (i.e. damping) increases when a building vibrates in the nonlinear range (inter-story strain above 10^{-3}). I don't know why, but it is commonly assumed that 5 % damping is a good assumption when designing an earthquake resistant building. In fact, the current standard relationships to predict response spectral amplitude as a function of distance and earthquake magnitude assume 5 % damping.

Damping of wooden houses

In order to see how damping affects the analysis of a building, I will consider the problem of a wooden house. I discussed wooden houses earlier in this chapter and I argued that they are very resilient in strong shaking. I argued that they are lightweight and that they have high stiffness to minimize deflections from the gravity load of contents (often called the live load). Forced vibration tests of wooden houses typically show that their fundamental mode resonance is about 7 Hz.

The California Earthquake Authority (CEA) sponsored a quantitative study of the vulnerabilities of wooden houses in earthquakes. They tested key structural elements to understand their yielding properties. There are numerous observations of wooden houses in strong shaking and collapse of foundation cripple walls is probably the most important class of failures. Cripple walls are short walls between the concrete foundation and the first-story floor (Figure 6.47 shows an example). Prior to building code updates in the mid-20th century, cripple walls were designed to provide a crawl space beneath a house, and they were designed tp support the vertical weight of a house; their lateral strength was often low. New houses are required to have cripple walls that are braced against

shear forces. Typically, cripple walls include plywood panels that resist in-plane shearing.

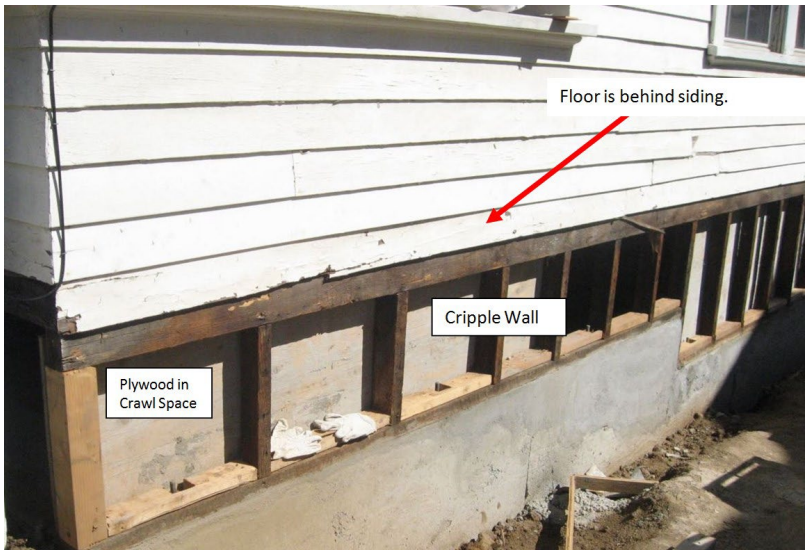

Figure 6.47. Example of a cripple wall on an old wooden house. The left end of the cripple wall has been retrofitted with plywood that resists shearing that is parallel to the wall. The solid wooden floor is strong and rigid and it ensures that there is no weak direction as long (as all the cripple walls are retrofitted).

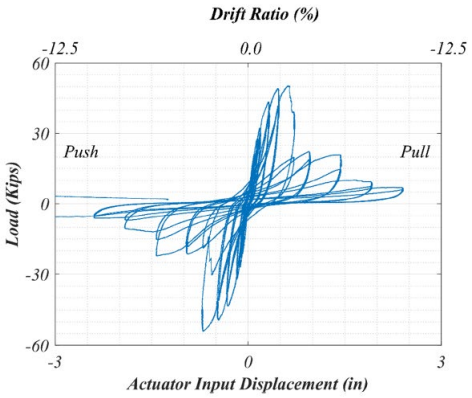

Figure 6.48. Force vs shear displacement for a cripple tested by the Pacific Earth Engineering Research Center (PEER) for the California Earthquake Authority (CEA). A hydraulic ram forces the cripple wall through a series of back and forth displacements whose amplitude grows with each cycle. As the wall is sheared, the force is also recorded. This shows the force displacement relationship for an unretrofitted cripple wall.

Figure 6.48 is the force/deflection curve for an unretrofitted cripple wall based on experimental test data. Note that the system is very far from elastic for any deflections more than 1.0 cm. While this system is also far from perfectly plastic, it can be thought

of as an elasto-plastic system (very approximately) with strains up to about 10% (deflection of 7 cm).

Before delving into nonlinear dynamics, I just want to remind everyone that the relation between maximum acceleration and maximum displacement of a 7-Hz harmonic oscillator is $\ddot{u}_{\max} = (2\pi \cdot 7\text{Hz})^2 u_{\max}$. So if the maximum acceleration is 1 g then the maximum displacement is 0.5 cm. That is, if the structure was oscillating at 7 Hz with a maximum displacement of 2.5 cm (about 1 inch), then the maximum associated acceleration would be on the order of 5 g. Clearly, the natural frequency of 7 Hz cannot apply to cripple walls that are deforming by an inch or more.

Figure 6.49 shows the envelope of the force/deflection cycles shown in Figure 1, and it is probably a good approximation to a static pushover analysis of the unretrofitted cripple wall. Since the point of the analysis is to characterize the vulnerability of old unretrofitted houses, I will focus on the dynamics of unretrofitted test specimens.

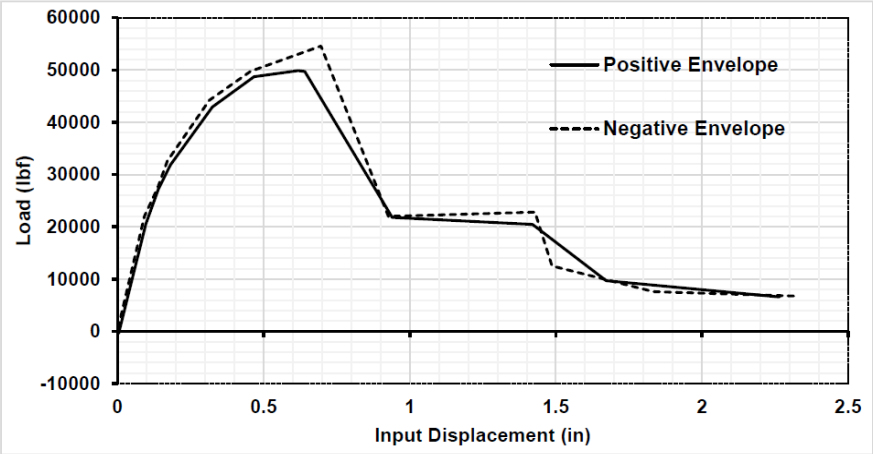

Figure 6.49 is also copied from the report of Working Group 4 and it shows that envelope of the force deflection curve in Figure 6.48.

Although an important objective of this study was to use experimentally consistent hysteretic models of force/deflection for dynamic analysis of wooden structures, I can gain some insight into the physics of the in-plane deformation of this cripple wall by using a very simple model of an elasto-plastic single degree of freedoom oscillator (sdof) that is driven harmonically (see Figure 6.50).

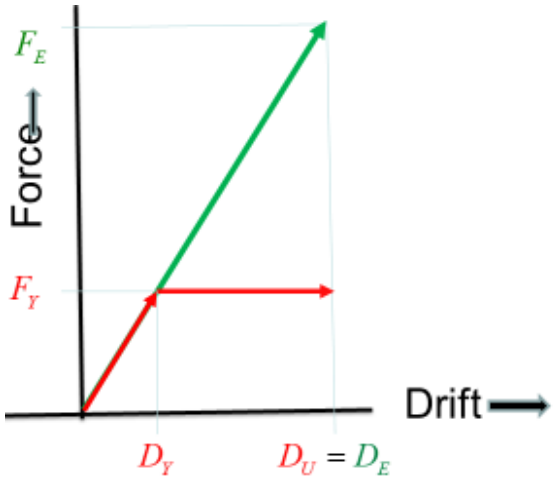

Figure 6.50. Definition of parameters for an elasto-plastic single-degree-of-freedom oscillator.

Consider an elastic-plastic single-degree-of-freedom oscillator with mass m, and a yield force F_Y that occurs when the deflection exceeds D_Y (see Figure 6.50). The elastic period of the sdof is

$$T_E = \frac{1}{2\pi}\sqrt{\frac{m}{k}} = \frac{1}{2\pi}\sqrt{m\frac{D_Y}{F_Y}} \tag{6.86}$$

Let D_U represent the maximum displacement of the system. If the deformation is large enough to yield the system, that is, if $D_U > D_Y$, then the approximate period of the plastic system is

$$\begin{aligned} T_P &= \frac{1}{2\pi}\sqrt{\frac{m}{k_P}} \\ &\approx \frac{1}{2\pi}\sqrt{m\frac{D_U}{F_Y}} \end{aligned} \tag{6.87}$$

where k_P is the equivalent (secant) stiffness of the elastic-plastic system. Now define the ductility of the system to be $R \equiv \frac{D_U}{D_Y}$, which is also sometimes called the "R-factor" in the design of elastic-plastic structures. In this case, D_U, is the maximum stable (i.e., ultimate) deflection of the system. Substituting into (6.87) shows that,

$$T_P \approx \frac{1}{2\pi}\sqrt{m\frac{RD_Y}{F_Y}} = T_E\sqrt{R} \tag{6.88}$$

That is, the plastic period increases as the square root of the ductility. In the case of Figure 6.49, the system shows strong strain-weakening behavior (progressive loosening of the nails) and the secant stiffness is more than a factor of 4 lower than for a perfectly plastic case. That is, for deflections greater than 4 cm (drift about 6%), the effective stiffness drops by more than a factor of 16, which would increase the natural period by a factor of 4. In the case of the PEER-CEA structures and drifts larger than 6%, $T_p \approx T_E R$.

That means that the effective period of these houses would drop from 0.15 s. to about 0.6 s. Or put in another way, when a typically stiff house is shaken strongly enough to produce damage, then its effective period lengthens to be similar to that of a typical six-story elastic building.

Although the change in effective period is important, the change in the effective damping is even more important. Linear damping is most commonly interpreted as viscous damping; it's a kind of energy dissipation where the total system energy steadily decreases by a fixed fraction with every cycle of vibration. In that case, the fraction of critical damping ς of an sdof can be approximated by estimating the energy lost to dissipation in a cycle (See Chapter 1).

$$\begin{aligned}\varsigma &\approx \frac{1}{4\pi}\frac{\text{Energy dissipated in a cycle}}{\text{Elastic energy in cycle}} \\ &= \frac{1}{4\pi}\frac{\text{plastic work in a cycle}}{\text{Elastic energy in cycle}} \\ &\approx \frac{1}{4\pi}\frac{\text{plastic work in a cycle}}{\text{maximum kinetic energy}}\end{aligned} \tag{6.89}$$

Using the perfectly plastic model of Figure 3, I can estimate the plastic work in a deformation cycle as four times the product of the yield displacement, $\left(D_U - D_Y\right)$, with the plastic yield force F_Y. I can also approximate the sum of the kinetic and potential energies in the cycle to be the maximum kinetic energy during the cycle (this is strictly true for a linearly elastic system in free vibration). I will estimate the maximum kinetic energy by assuming that the maximum velocity of the mass is approximately the maximum displacement divided by the plastic period, or $\dot{x}_{\max} \approx 2\pi\left(\frac{D_U}{T_P}\right)$. (6.89) can then be rewritten as

$$\varsigma \approx \frac{1}{4\pi}\frac{4\left(R-1\right)D_Y F_Y}{\frac{1}{2}\mathrm{m}\dot{\mathrm{D}}_U^2}$$

$$\begin{aligned}&\approx \frac{1}{4\pi}\frac{4\left(R-1\right)D_Y F_Y}{\frac{1}{2}\mathrm{m}\left(\frac{2}{\pi T_P}D_U\right)^2} = \frac{T_P^{\,2}}{\pi}\frac{\left(R-1\right)D_Y F_Y}{2\mathrm{m}\mathrm{D}_U^2} = \frac{T_P^{\,2}}{\pi}\frac{\left(R-1\right)F_Y}{2\mathrm{m}\mathrm{R}^2\mathrm{D}_Y} \\ &= \frac{T_P^{\,2}}{\pi}\frac{\left(R-1\right)}{2\mathrm{m}\mathrm{R}^2}\frac{m}{T_E^2} = \left(R-1\right)\frac{1}{2\pi}\left(\frac{T_P}{T_E}\right)^2 \\ &\approx \frac{R\left(R-1\right)}{2\pi}\end{aligned} \tag{6.90}$$

(6.91)

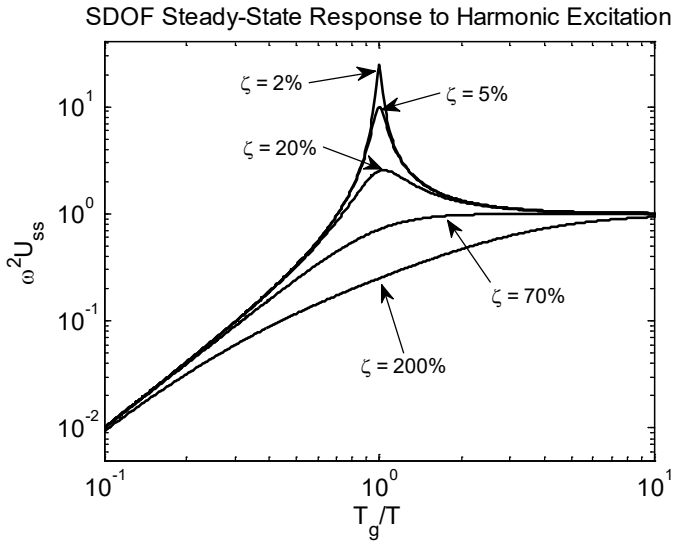

Figure 6.51. Response curves for different damping. There is no resonant peak for damping greater than 71% of critical. Notice that the slope of the log (acceleration response) vs log (period) is approximately linear with increasing driving period. This means that amplitude of the displacement response (i.e, the drift) scales linearly with ground velocity. Also, notice that when the damping is very large, the natural period of the oscillator is not very important. That is, the higher the damping, then the broader the frequency range that response measures velocity.

As we go to large ductility and long driving period, the fraction of critical damping goes way up. In fact, for the hysteretic loops shown in the CEA Wood report, the system is effectively overdamped. If the ductility in a damaging earthquake is 6.0, then the effective plastic period of a 0.2-s house would increase to about 0.8 s. That means that driving periods longer than 0.5 s would have the most importance to cause plastic drift. In this case the fraction of damping would be about 400%. While I admit that this is a very crude approximation, it seems clear to me that the effective damping is very large.

Lightly-damped systems (e.g. 5%) have peak responses that are relatively insensitive to the phase spectrum of the driving force (the ground acceleration); that is, for lightly damped response spectra, it doesn't matter too much whether all of the energy arrives in one pulse or whether the energy arrives randomly throughout the time period. Of course, the phase does have some influence response spectra; otherwise, we would use Fourier amplitude spectra.

Figure 6.51 shows the response curves of linear sdof's for different damping. As an example of the importance of damping, consider that modern seismometers are designed to be 71% damped sdof's. This is chosen so that there is no resonance at any period, thereby optimizing the bandwidth of motions that the seismometer records. This 71% damping also means that seismometers do a good job of recording seismic phases, which tend to arrive as pulses. Here is the thing about time-domain pulses, a pulse is inherently

a broad-band phenomenon; pulses occur when a wide range of frequencies arrive in phase.

The use of highly damped response spectra to characterize motions that damage ductile buildings was suggested by Shiyan Song in his 2013 Caltech PhD thesis. Figure 6.52 is taken from his PhD thesis (Song, S., 2013, A New Ground Motion Intensity Measure, Peak Filtered Acceleration (PGA), to Estimate Collapse Vulnerability of Buildings in Earthquakes, Ph.D. Thesis, California Institute of Technology, Pasadena, CA.) and it shows a comparison between a variety of parameters and the base shear force in a simulated 6-story Steel MRF that is experiencing strong plastic yielding. This figure was the outcome of incremental dynamic analysis. That is, the input ground acceleration was scaled to be just large enough to cause collapse ($P-\Delta$ instability). The top five traces are all on the same scale (force/weight, or % g). The second (yellow) trace is a 2%-damped sdof at the natural frequency of the building; the peak of this trace is identical to the response spectral acceleration for the record that is shown in the top (blue) trace. The true base yield force is the red trace. Notice that this base shear looks like a low-pass filtered version of the acceleration. Further, notice that the amplitude of the base shear (the red trace) is limited to be less than 23% of the weight of the building (this is the plastic pushover yield stress). Finally, the purple trace is a linear sdof with a natural period of 1.5 times the elastic period and with 71% damping. Notice that the purple and red traces are very similar when there is significant structural yielding. This result is anticipated by equations (6.86) and (6.88). This example shows why strong damping is a better way to parameterize strong shaking than is 5% damping. Coincidentally, the procedure for calculating a 71 %-damped response spectrum is identical to finding the maximum amplitude of a ground motion record that has been low-pass filtered with a 2-pole Butterworth filter (see Chapter 2). Therefore, Sang referred to his damage parameter as *peak filtered acceleration* (pfa)

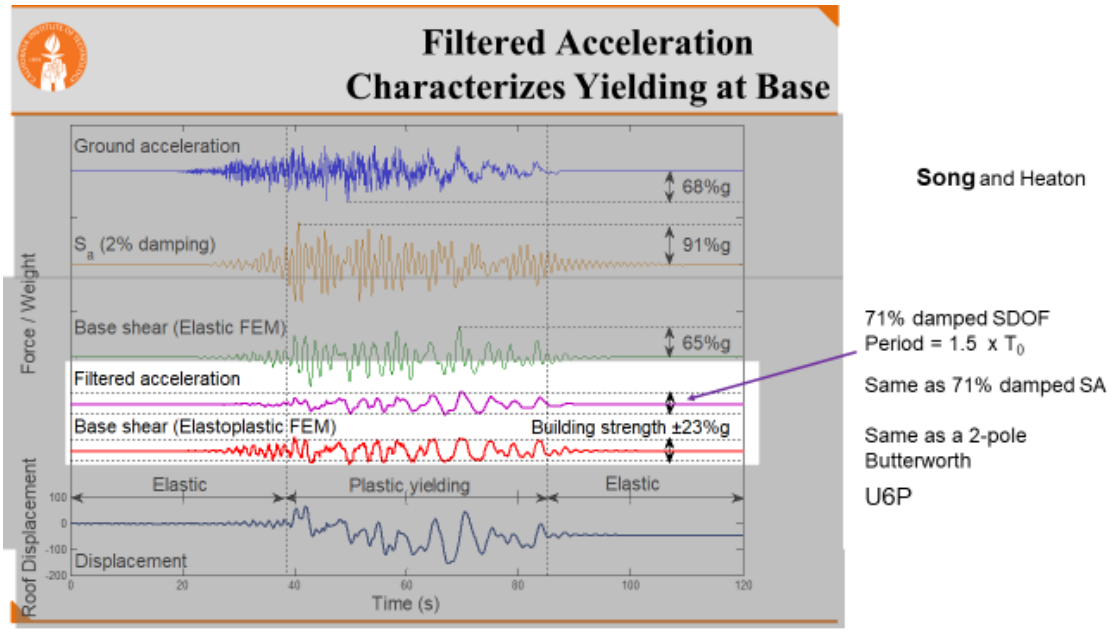

Figure 6.52. Is from the PhD dissertation of Shiyan Song (2013, Caltech) and it compares different time series that describe the response of a 6-story steel MRF building that experiences large plastic deformation (just smaller than $P-\Delta$ collapse). Whenever appropriate, all traces are on the same acceleration amplitude scale. The second (yellow) trace is the mass acceleration of a 2% damped linear sdof with the elastic free period of the building. The red trace is the base shear force of the yielding building given as a % of its weight. This base shear stress is limited to 23% of g, which is the plastic yield stress derived from push-over analysis.

Based on this insight, Song developed a procedure to predict the $P-\Delta$ collapse of buildings using parameters derived from a pushover analysis. Using full nonlinear analysis of steel mrf's, tested which simple parameters best predicted collapse reported by the complex analysis, He used a procedure called incremental dynamic analysis. In this procedure, a ground motion is used to compute the nonlinear response of a building model. The ground motion is then increased by a scale factor and the nonlinear response is calculated again. This procedure is repeated until the ground motion is large enough to cause simulated $P-\Delta$ collapse. This subject is more completely described in a recent paper by Buyco and Heaton (2019, 70%-Damped Spectral Acceleration as a Ground Motion Intensity Measure for Predicting Highly Nonlinear Response of Structures, Earthquake Spectra 35 (2), 589-610).

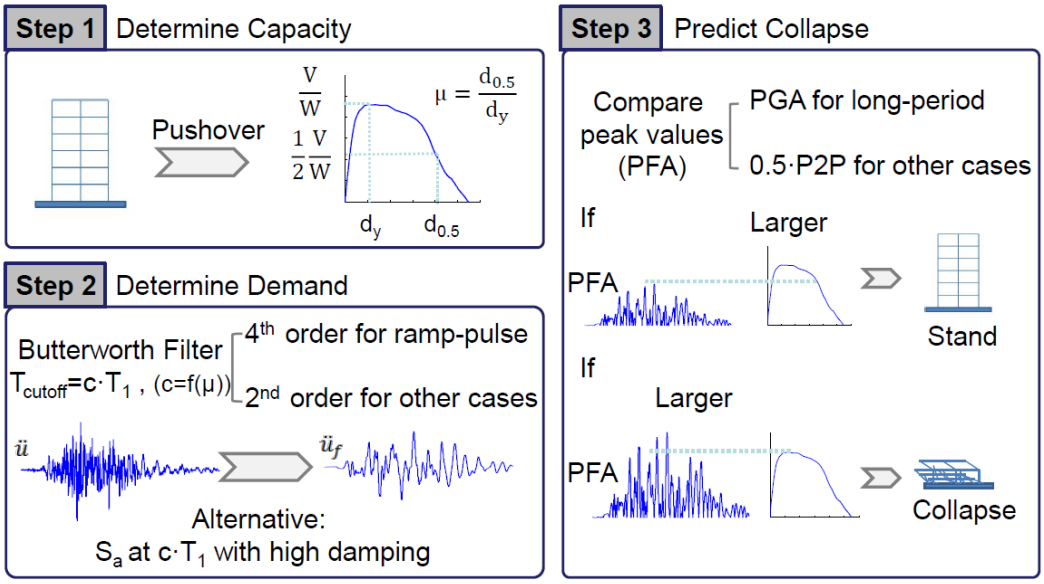

Figure 6.53 Procedure to predict the $P-\Delta$ collapse of a building from a nonlinear pushover analysis. The procedure is slightly different for motions that are dominated by a step in ground displacement.

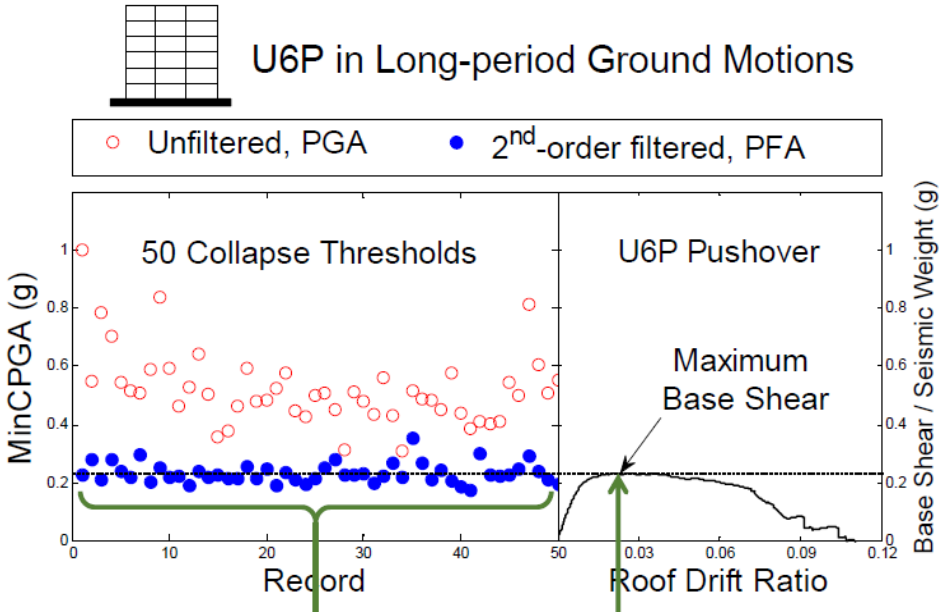

Figure 6.54 From Song's PhD dissertation. Vertical axis is horizontal acceleration in g. The red dots are peak accelerations of records that were just large enough to cause $P-\Delta$ collapse. The blue dots are the peak accelerations of the same records after filtering with a 2nd order low-pass Butterworth with a corner period of 1 ½ times the natural period. This is identical to 71% damped response spectral acceleration. The graph on the lower right shows the nonlinear pushover curve for the building. Notice that the amplitudes of the filtered accelertions that cause collapse are close to the peak static pushover acceleration of the building.

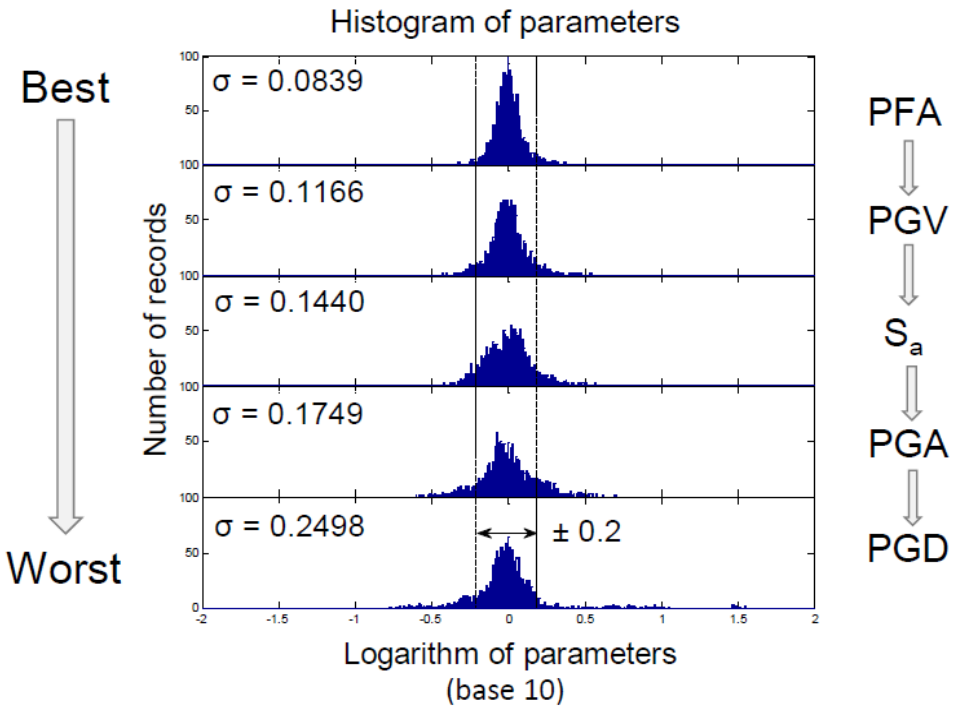

Figure 6.55 Dispersion of intensity measures that caused simulated collapse of a 6-story steel MRF. The intensity measures are ordered from best performance to worst. Increasing the damping to 71% (Peak Filtered Acceleration, PFA) decreases the dispersion by almost a factor of 2. σ is the standard deviation of the log normal distribution fit to each correlation.

Song's dissertation shows a formalism for predicting the collapse of yielding buildings based on 71 % damped response spectra. Figure 6.55 shows the amplitudes of a variety of intensity parameters for several hundred ground motions that were large enough to induce $P-\Delta$ collapse. This study used an incremental dynamic analysis of collapse ($P-\Delta$ instability).

Although 71% damped S_a at 1.5 times the natural period is the best predictor, pgv is a reasonable alternative to 71% damped spectra. This is verified in Song's study of collapse parameters (Figure 6.55). That is, pgv is the second-best intensity measure.

The correlation of damage (primarily to wooden houses) and pgv was also studied by Wald, Quitoriano, Heaton, and Kanamori (Spectra 1999). Modified Mercalli intensities (MMI) determined from observations of damage at particular sites was plotted against both pga (Figure 6.56) and pgv (Figure 6.58) for accelerograms recorded less than 3 km from the damaged structure. There is a lot of scatter in these plots and one could easily despair that there is nothing important to see. However, from the point of view of understanding structural damage, I believe that there is something to be learned from the sites that experienced MMI of VIII or greater. Sites that experience significant cripple wall damage would be assigned MMI's of VIII or greater. Notice that in Figure 6, the median pga for VIII and IX is virtually the same (about ½ g). Importantly, ½ g is the

level of saturation of pga for all crustal earthquakes and it occurs primarily in the very near-source region (Joyner-Boore distance < 10 km) of earthquakes larger than M 6. For example, Figure 7 shows all available pga's from very near-source stations in M>6 earthquake (as of about 2005). These data are well described by a log-normal distribution with a geometric mean of 47% g.

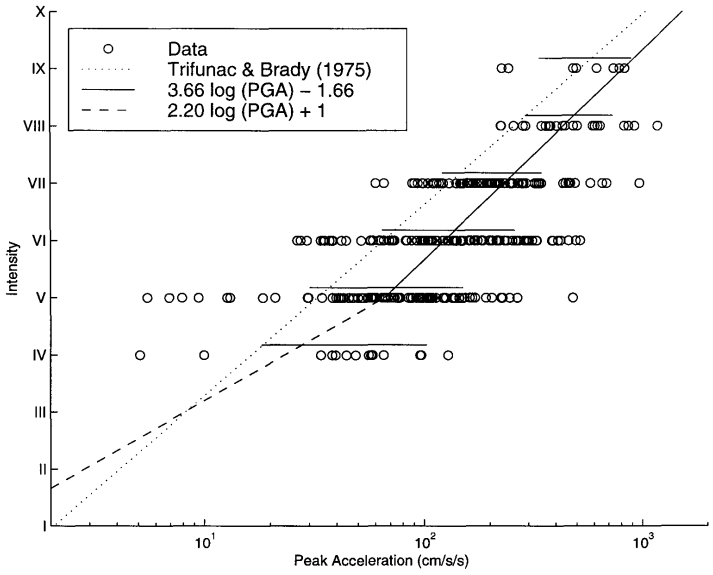

Figure 3. Modified Mercalli intensity plotted against peak ground acceleration for all events combined. Circles denote data; horizontal lines above data depict the range of the geometric mean, plus and minus one standard deviation. The solid line is regression from this study, the dashed line is assigned (see text for details). The dotted line is that of Trifunac and Brady (1975).

Figure 6.56 This is copied from Wald, Quitoriano, Heaton, and Kanamori (Spectra, 1999).

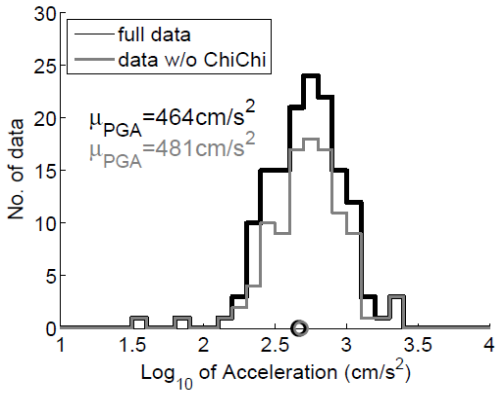

Figure 6.57. This is copied from Yamada, Olsen, and Heaton and it shows the pga for all near-source recordings (JB distance less than 10 km) of earthquakes larger than M 6 for all available data at the time of publication (2004). The grey histogram includes all data prior to the M 7.7 1999 Chi-Chi earthquake, and the black histogram includes the Chi-Chi data. Notice that the addition of Chi-Chi data had a neglibable effect on the geometric mean. That is pga saturates at a geometric mean of about ½ g; It seems likely that near-source pga from future earthquakes will also be log-normally distributed about ½ g.

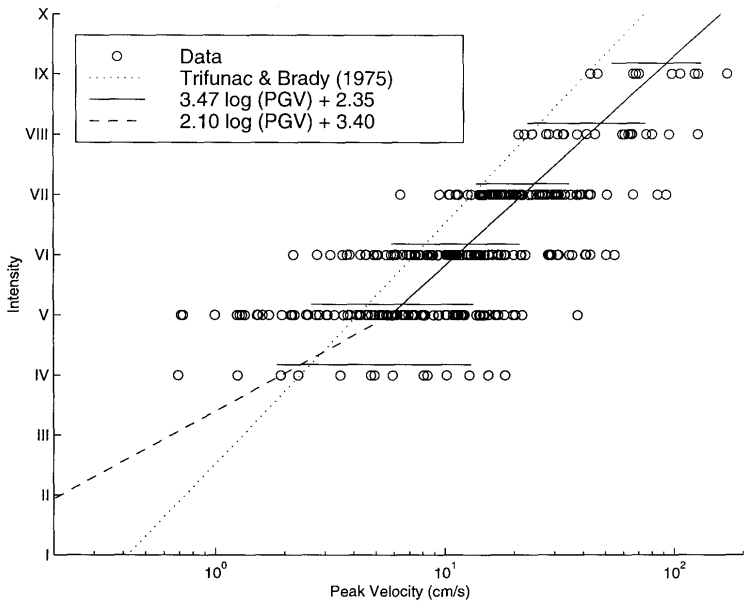

Figure 4. Modified Mercalli intensity plotted against peak ground velocity for all events combined. Circles denote data; horizontal lines above data depict the range of the geometric mean, plus and minus one standard deviation. The solid line is regression from this study, the dashed line is assigned (see text for details). The dotted line is that of Trifunac and Brady (1975).

Figure 6.58. Same as Figure 6.56, but for pgv.

In contrast, Figure 6.58 is the same as Figure 6.56, but for pgv. Notice that the median pgv for intensity IX is about 100 cm/s, whereas it is about 40 cm/s for intensity VIII. This is clear evidence that pgv is a better predictor of damage to wooden houses than pga is (or 7 Hz response spectral acceleration).

Reason for the Importance of pgv

During the early part of my career, peak ground acceleration (pga) was considered to be the most important measure of shaking intensity. There were lengthy debates about whether or not pga could exceed 1 g. We now have numerous well documented cases where the acceleration was substantially larger than 1 g. Interestingly, the damage to buildings adjacent to high acceleration records has typically been minor. It has long been noted that high peak ground velocity (pgv greater than 1 m/s) is very damaging to buildings. This observation has often been viewed as counter intuitive; doesn't $f = m\ddot{a}$? Not really; $f = m\ddot{a}$ only applies to rigid bodies (or alternatively it applies when a is the acceleration of the center of mass).

I will now describe another way to understand why pgv is important for damaging buildings. Start with the equation of motion for a linear sdof

$$\ddot{u} + \ddot{x} + 2\omega_0 \varsigma \dot{x} + \omega_0^2 x = 0 \tag{6.92}$$

Where u is the ground motion (displacement), x is the motion of the mass relative to the base of the spring, ς is the fraction of critical damping, and ω_0 is the natural frequency of the undamped oscillator. When the damping becomes large, then the dissipation energy becomes large compared with the elastic energy in the spring. That is $\omega_0^2 x$ becomes smaller than other terms and (6.92) can be approximated (very roughly) as

$$\ddot{u} + \ddot{x} + 2\omega_0 \varsigma \dot{x} \approx 0 \tag{6.93}$$

Integrating with respect to time gives

$$\dot{u} + \dot{x} + 2\omega_0 \varsigma x \approx 0 \tag{6.94}$$

Now we want to find the maximum of x over time (the maximum drift). When x is a maximum, then $\dot{x} \approx 0$, and so

$$\dot{u}_{\max} + 2\omega_0 \varsigma x_{\max} \approx 0 \tag{6.95}$$

Or

$$x_{\max} \approx \frac{1}{2\omega_0 \varsigma} \dot{u}_{\max} \tag{6.96}$$

That is, we **expect the maximum drift of the plastic sdof to approximately scale with peak ground velocity**. This is consistent with my remarks in Figure 6.51 about the characteristics of the response of a linear sdof.

It amazes me that there still seems to be considerable attention given to pga and its related parameter, high-frequency response spectral acceleration. These parameters are widely thought to be important for nuclear power stations. Nuclear power stations are usually comprised of massive reinforced concrete shells and diaphragms that are exceedingly stiff. Although these structures are designed for much larger loads than what happens in earthquake shaking, the mechanical equipment that controls the station (e.g., pipes, pumps, motors, etc.) could be vulnerable. Personally, I think that it is best to invest in quality bushings and shock mounts that isolate critical equipment from high frequency shaking. That is, I am very skeptical that high frequency shaking is a significant problem.

Figures 6.59 and 6.60 show the median behavior of near-source (rupture distance less than 5 km) pga and pgv as a function of earthquake magnitude. A variety of different studies are shown. It seems pretty clear that near-source pga saturates fully as a function of magnitude. In contrast, pga shows a change in the magnitude scaling at about M 6 ½, but it does not appear to fully saturate.

As is often the case, the things that matter the most are also the things that we know the least about. Since the time of the creation of the gmpe's shown in Figures 6.59 and 6.60, there have been a number of new large earthquakes around the World. Table 6.2 shows pga, pgv, and pgd from near-source records from recent large earthquakes. Clearly, future earthquakes will provide a new wealth of records with impressively large pgv's and pgd's. The column labeled as tilt is the size of a step in tilt during strong shaking that makes the double integration of acceleration a stable procedure (see Chapter 2).

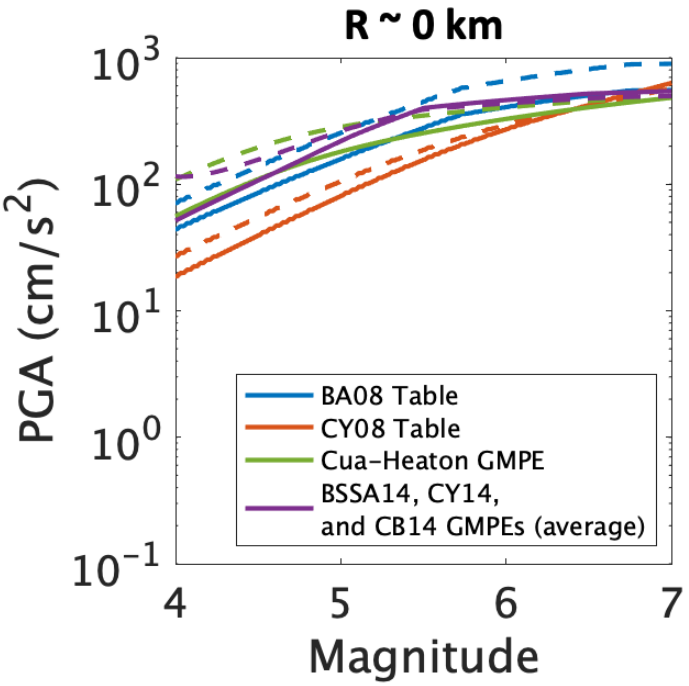

Figure 6.59. A variety of ground motion prediction equations (gmpe's) that show the best fit of near-source pga data as a function of magnitude. The Cua-Heaton and relationships with a 14 are the most recently published.

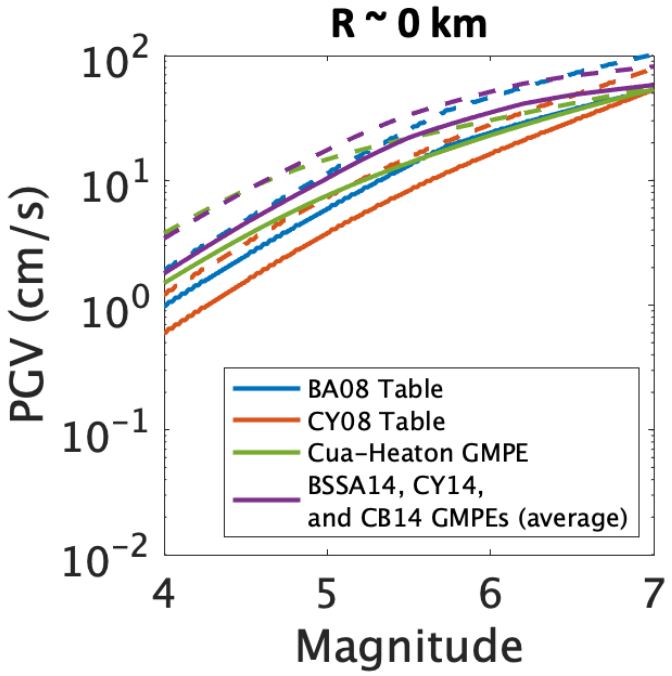

Figure 6.60. A variety of ground motion prediction equations (gmpe's) that show the best fit of near-source pgv data as a function of magnitude.

Design Response Spectra

5 % damped response spectra are typically very complex functions of period (or frequency). They are thought to provide estimates of the base shear stress for the fundamental mode. The fact that the spectra vary so strongly makes it difficult to determine a shear strength that is appropriate for the design of buildings. In reality, the narrow-band peaks really only apply to linear oscillators; nonlinear oscillators shift their resonance frequency as the amplitude increases. Furthermore, it's low damping that makes for resonant peaks in the first place.

In order to actually use response spectra for the design of buildings, seismic building codes use response spectra that are smoothed version of actual spectra. These spectra are not only smoothed, but they are decreased in amplitude because designers believe that buildings can withstand drift displacements that far exceed the displacement at which the building will begin to yield. Designers used this principle to introduce the **R-Factor** (or reduction factor) into building codes. They argued that buildings could survive drifts that were up to ten times larger than the drift at wich the building begins to yield. Since the designws were based on linear modal analysis, they argued that response spectrum that should be assumed for design should not only be a simple smooth function, it should also be much less than observed response spectra that assume linear sdof's.

Figure 6.61 shows the response spectra of ground motions that were just large enough to cause $P-\Delta$ of a simulation of a six-story steel mrf. These spectra are shown for both 5 % damping (red) and also 71 % damping (black), which is the same as a low-pass Butterworth filter. This figure is from Song's dissertation and it shows that use of 71 % damping produces spectra that are much more similar to the standard design spectrum (blue). When comparing the 71 % damped spectra to the standard design spectrum it's important to remember that the building's effective period should be 1.5 times that of the period used for the standard design spectrum.

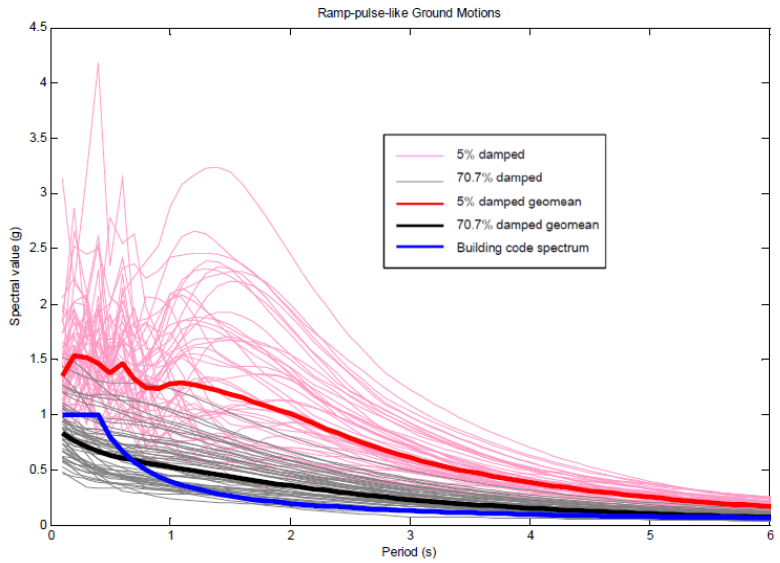

Figure 6.61 These are the response spectra of the 50 scaled records that were just large enough to cause $P-\Delta$ collapse in Song's study (see Fig. 6.54). The red curves assume the industry standard of 5 % damping, whereas the black curves assume 71 % damping. The heavy lines are the geometric means of the individual curves. The solid blue line is the spectral acceleration specified for the design of California buildings in high hazard regions.

Role of Peak Ground Displacement

There is yet another way to understand the vulnerability of buildings to $P-\Delta$ collapse. That is, there are two conditions that must occur for collapse. First, the building must experience inter-story plastic yielding, and second, the inter-story displacements must be large enough that the building is $P-\Delta$ unstable. In particular, we can anticipate that 1) pgv must be large enough to cause elastic waves with large enough strains to cause yielding and 2) that simultaneously pgd must be large enough to make the building unstable.

As an example, I will return to the models of six- and twenty-story steel frame buildings. Pushover curves for variations of these buildings (e.g., US code and Japanese code) are shown in Figure 6.62. Notice that the Japanese code buildings have considerably larger yield strength than the comparable US code buildings. Also notice that the largest roof drift of both 20-story buildings is a little over 2 m. That is, these buildings are gravitationally unstable if the roof moves more than 2 m with respect to the base.

Anna Olsen did a full nonlinear finite element analysis on these buildings using 45,000 synthetic records of ground shaking that assumed a variety of rupture models for earthquakes as large as M 7 ¼ (Olsen, Heaton, and Hall, Spectra). These simulated ground motions were the result of a large collaborative project by the Southern California Earthquake Center (SCEC). The SCEC motions were low-pass filtered at 0.5 Hz (these were band-limited finite element models). Actual records with similar low-frequency amplitudes have pgv's that are about 50 % larger than those in this study.

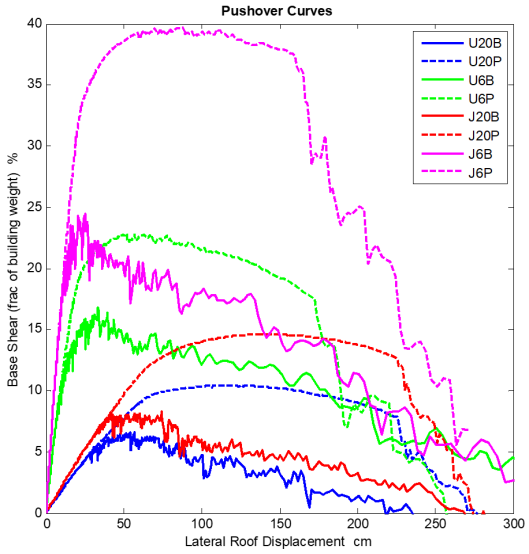

Figure 6.62. Data from simulations of the U20P building model response to long-period ground motions in the S_a-ε (top row), PGD_{lp}-PGV_{lp} (middle), and PGD_{bb}-PGV_{bb} (bottom) planes. The building responses are: "standing" or "collapse" (left column) and "repairable" or "unrepairable" (right)

Each of the 45,000 nonlinear simulations of the 20-story, US-buildings is represented by a dot in Figure 6.53. The location of each dot shows the filtered pgv and the broad-band pdg for each record. If the beams in the simulations have a permanent plastic strain of less than 8×10^{-3}, then the building is represented by a grey dot and it is called repairable. If the building experiences a side-sway collapse, then the dot is red. Finally, if the building is permanently bent more than 8×10^{-3}, but it doesn't collapse, then the dot is black and the building is called unrepairable.

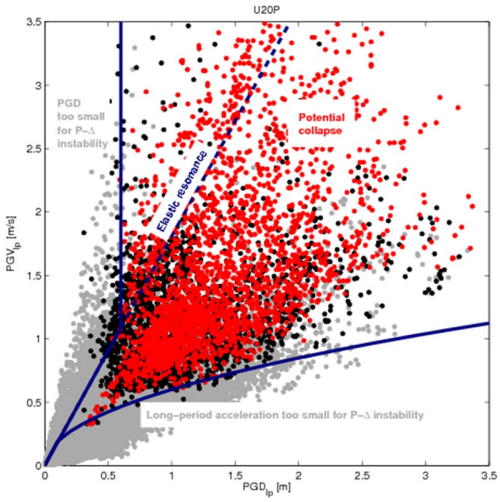

Figure 6.63 responses are: "standing" or "collapse" (left column) and "repairable" or "unrepairable" (right).

Notice that the red dots are generally in the upper right of the plot. Most collapses happen when pgv>60 cm/s **and** pgd > 60 cm. Remember that when an upward traveling shear wave reflects off the roof, the amplitude of the roof displacement is twice that of the ground displacement. That is, a pgd of 60 cm should produce a roof drift of about 120 cm, which is getting the near limit for $P-\Delta$ stability. The diagonal dotted line called elastic resonance is $pgv = \omega_0 pgd$, where $\omega_0 = 2\pi/T_0 = 1.8\,\text{radians}/s$. Notice that most of the collapses occur to the right of this line. That is, pgd is a very important parameter when it comes to collapse of tall buildings.

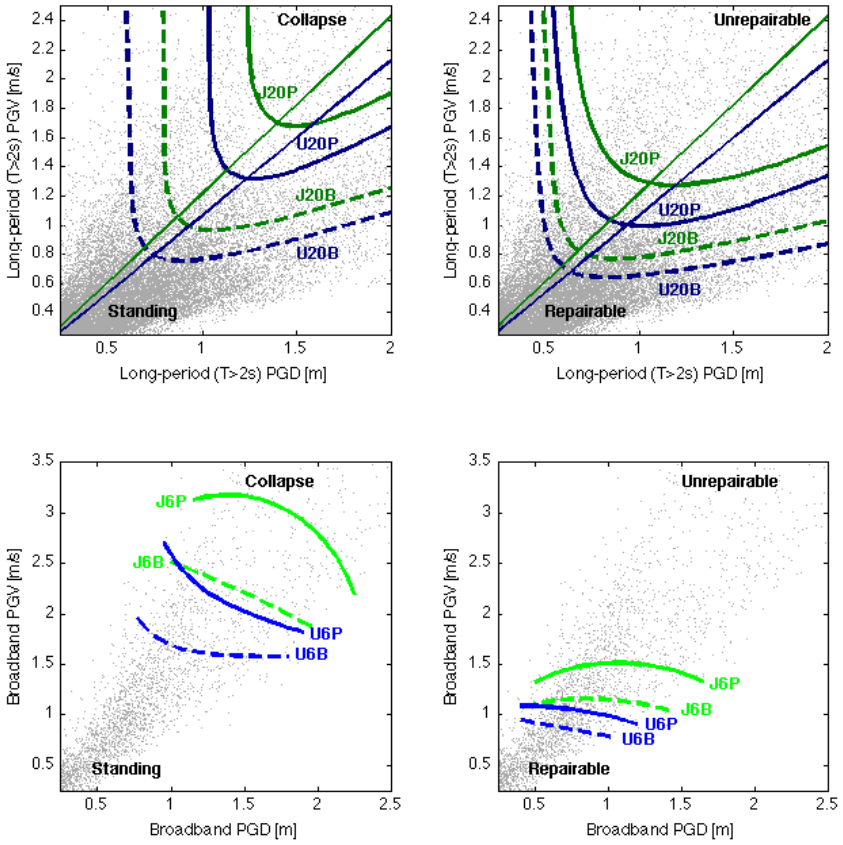

Figure 6.64. Contours where the probability of "collapse" (left) or "unrepairable" (right) is 30%. The gray points are the PGD and PGV values of the long-period (top) and broadband (bottom) ground motions. The equivalent PGV_{bb} is approximately $1.5 \cdot PGV_{lp}$ with a standard deviation of 0.24 m/s. The diagonal lines in the top plots are $PGV_{lp} = \frac{2\pi}{1.7 \cdot T} PGD_{lp}$, where T is the fundamental elastic period of the J20P or U20P building model.

Anna Olsen ran this same analysis for the Japanese code buildings and also for buildings with brittle welds. Figure 6.64. shows lines of pgv vs pgd that separate regions of collapse from regions of no collapse. The diagonal resonance line for the Japanese buildings are slightly steeper because the Japanese code results in a stiffer building ($T_0 = 3.0$ s for the Japanese design as opposed to $T_0 = 3.5$ s for the US). Notice that brittle welds greatly decrease the collapse resistance of both US and Japanese designs. Also notice that the Japanese code results in a substantially better building than the US design.

I really like the clarity provided by Figure 6.64. It allows us to see what is the better design. Throughout much of my professional life, there was a debate about the merits of the Japanese building code vs the US building code (the Uniform Building Code, UBC). Many of my colleagues argued that while the Japanese code seems to produce a stronger building, it comes with the penalty that it is so stiff that it has higher forces than comparable US code buildings. Figure 6.64 seems to clearly settle that debate; you are more secure in Japanese code buildings. Unfortunately, most Japanese steel frame buildings built before 1995 have brittle welds (that is before the Northridge and Kobe earthquakes).

The bottom panels of Fig. 6.64 how the comparable analysis, but the buildings are all 6-story steel mrf's. Because the 6-story buildings are shorter period, the pgv values are increased by 50% to account for the fact that actual pgv from broadband records are larger than the pgv's from low-pass filtered records. Although both pgv and pgd are important for collapse of the 20-story buildings, pgv is the key parameter for the 6-story building. Again, the Japanese code building performs better than the US code building.

Table 6.2 is copied from Buyco, Roh, and Heaton. This paper discusses how standard signal processing of accelerograms can decrease the likelihood that the record will cause simulated collapse of long-period building designs. The table lists records from many large earthquakes as well as estimates of the true pgv and pgd. Notice that there are numerous examples of recorded pgv > 1 m/s and pgd > 1 m.

Earthquake	M	Station	R_{JB}	PGA (g)	PGV (cm/s)	PGD (cm)	Tilt (°)
		CULC	15.6	0.27	29	75	0.62
		KEKS	3.0	1.97	269	867	1.54
2016 Kaikōura	7.8	KIKS	0.7	0.51	160	304	1.83
		WDFS	8.5	2.51	210	816	1.23
		WIGC	18.0*	0.75	64	52	2.73
		WTMC	0.7	1.12	117	284	0.01
		93048	0.6	0.79	264	186	0.58
		93051	0.5	0.84	178	105	0.48
		KMM001	5.0*	0.22	39	45	0.58
		KMM004	3.9*	0.35	82	74	0.12
2016 Kumamoto	7.0	KMM005	5.6	0.54	69	115	0.55
		KMM007	3.5*	0.43	44	40	0.27
		KMM009	2.2*	0.79	38	41	0.19
		KMMH16	0.5	1.18	142	228	0.08
		OIT009	7.8*	0.73	78	102	0.11
2015 Gorkha	7.8	KATNP	0.1	0.16	112	246	0.02
		AXT	9.8	0.29	31	105	0.04
2008 Wenchuan	7.9	MZQ	0.8	0.82	136	213	0.07
		SFB	4.8	0.58	81	318	2.04
2002 Denali	7.9	PS10**	3.0	0.33	137	302	–
		TCU052	1.8	0.45	225	740	–
		TCU065	2.5	0.79	135	198	–
1999 Chi-Chi	7.6	TCU067	1.1	0.50	100	191	–
		TCU068	3.0	0.51	298	885	–
		TCU084	11.4	1.00	118	251	–
1992 Landers	7.3	LUC**	2.0	0.76	146	263	–

* Epicentral distance is reported because R_{JB} is not available.
** Two horizontal directions are oriented parallel and normal to the ruptured fault.

Table 6.2. This table is copied from Buyco, Roh, and Heaton (2020, Spectra) and it lists the pga, pgv and pgd for near-source observations of earthquakes larger than M 7.

Figure 6.65 is from a study by Aagaard, Heaton, and Hall and it shows the median pgd as a function of distance from the surface projection of the rupture area of simulate M 7 earthquakes. This figure shows that a good rule of thumb is that the area directly above the rupture has a median pgd that is about 2/3 the average slip on the fault. The vertical scale is pgd per unit of average slip on the fault. Average slip scales as $10^{\frac{1}{2}M}$. That is, average slip increases by a factor of 3 for every unit increase in M. While table 6.2 has some very large pgd values, there are numerous examples of historic earthquake fault scarps that imply much larger pgd's.

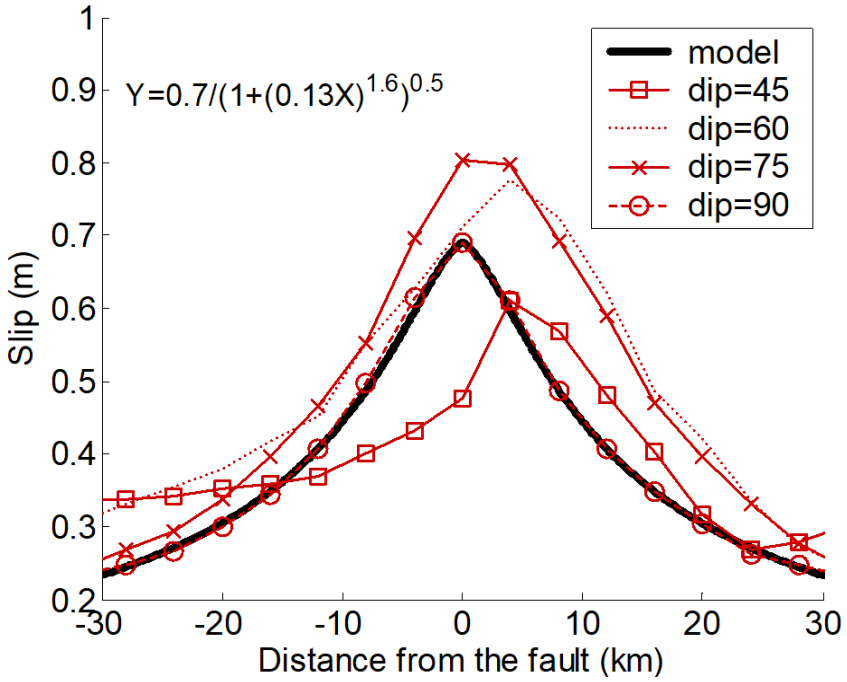

Figure 6.65.

Japan vs US buildings

It's one thing to compare simulations of buildings that comply with different building codes and quite another thing to compare the actual performance of buildings in real earthquakes. I have visited Japan many times and I am always impressed when I see Japanese buildings that are under construction. They appear quite different to US buildings. In particular, Japanese steel construction often uses rectangular box sections for columns. This means that all sides of a column are flanges that can be used to construct a moment-resisting connection. It is common to see Japanese buildings in which all beam-column connections are moment resisting. In contrast, US construction typically uses I-sections for columns. That means that moment resisting connections can only be constructed in one direction. The net result is that there are far fewer moment resisting connections in a US building than in a comparable Japanese building.

Part of the story of the difference between US and Japanese buildings has to do with the building code. You might think that these codes are written similarly, but with different constants in the code. In fact, these codes are a set of complex rules and it's difficult to anticipate the characteristics of the resulting building until you go through the process of checking a design to ensure that it meets all of the code requirements. Personally, I find the details of building codes to be impenetrable. Fortunately, I have collaborated with colleagues (Prof. John Hall, Prof. Swaminathan Krishnan, Dr. Kenny Buyco) who have the patience and skill required to produce models that meet building codes. In the US, most structural engineering firms that design earthquake-resistant buildings aspire to produce designs that meet code requirements, but they also try to minimize construction costs by specifying designs that exceed code requirements. Importantly, US cities have not been subjected to large near-source shaking (large pgv, pgd) since the 1906 San Francisco earthquake. In contrast, Japan experiences earthquakes at a rate that is roughly ten times higher than the west coast of the US. This means that Japanese buildings have

been tested in the real world more frequently than US buildings. As a result, Japanese engineers are usually more cautious than US engineers.

In my view, the most important difference is that Japanese buildings are typically developed by a company that coordinates all of the aspects; architecture, geotechnical engineering, structural design, construction, and long-term maintenance is often handled by the same company. For example, Shimizu and Kajima are large construction companies that take a building from design to operation. These companies are proud of their buildings and they openly show the buildings that are their product. If one of their building was destroyed by an earthquake, then this would be viewed as an embarrassment that would damage the reputation of the company. It is my view that many Japanese buildings exceed the required code to ensure the long-term viability of these construction companies.

Chile – a different approach

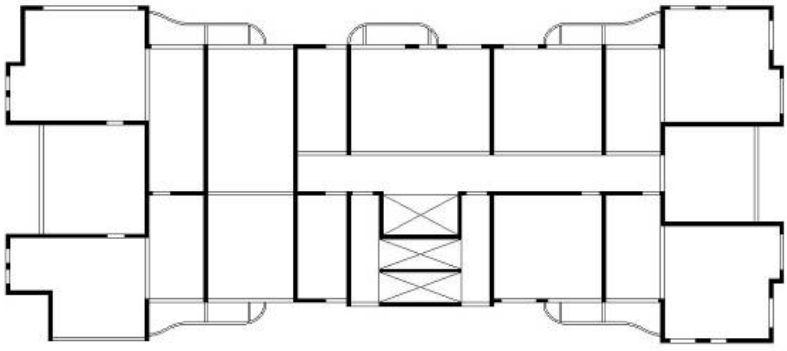

Shear failure in a new 25-story shear wall building in the 2010 Maule earthquake

Collapse of a shear wall building in the 2010 Maule earthquake

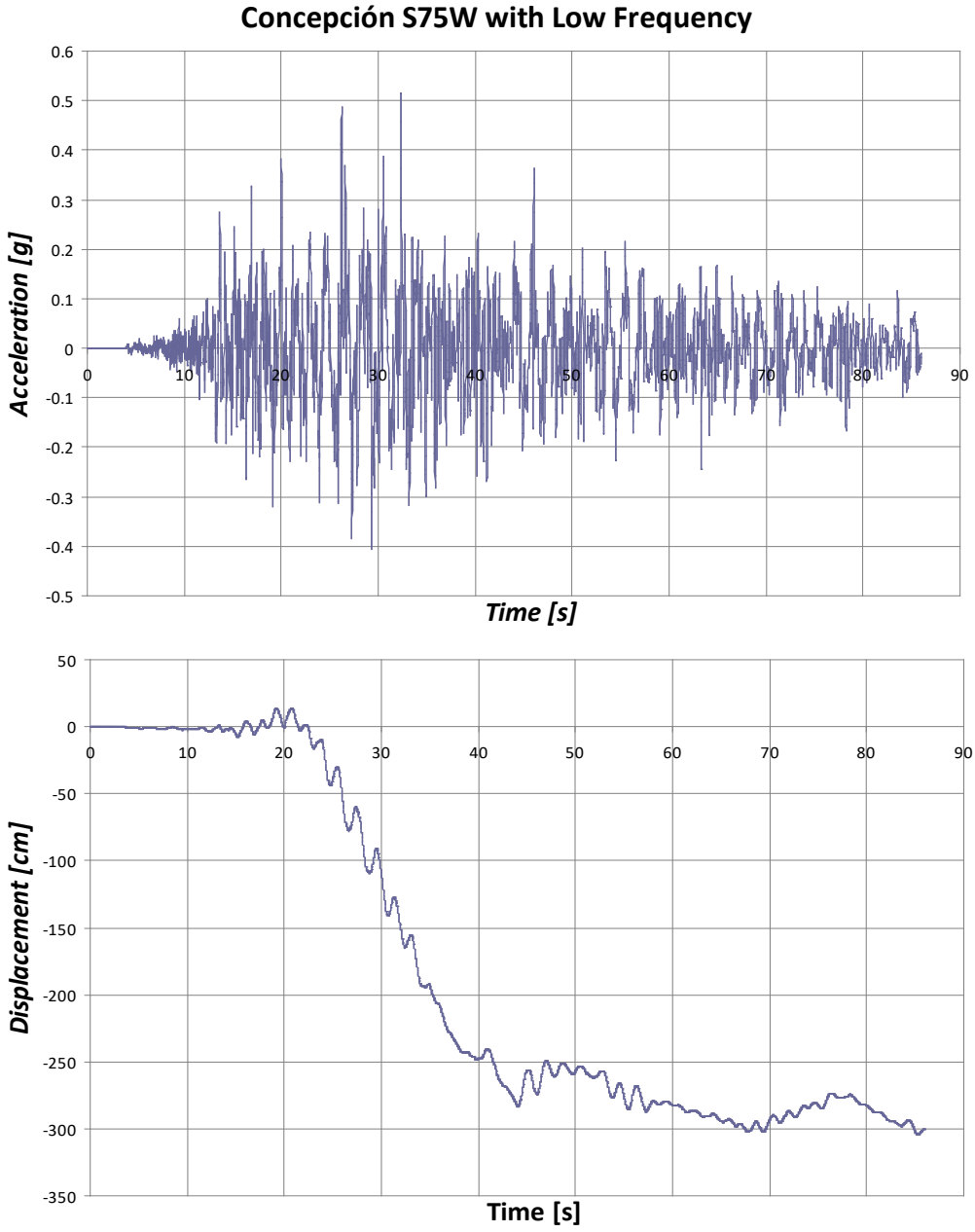

Core wall buildings

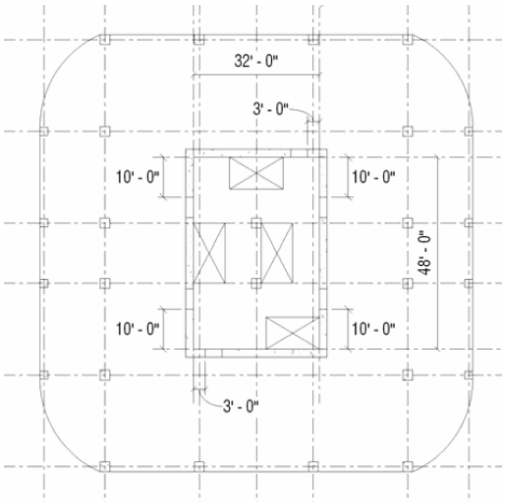
32' - 0"
3' - 0"
10' - 0"
10' - 0"
48' - 0"
10' - 0"
10' - 0"
3' - 0"

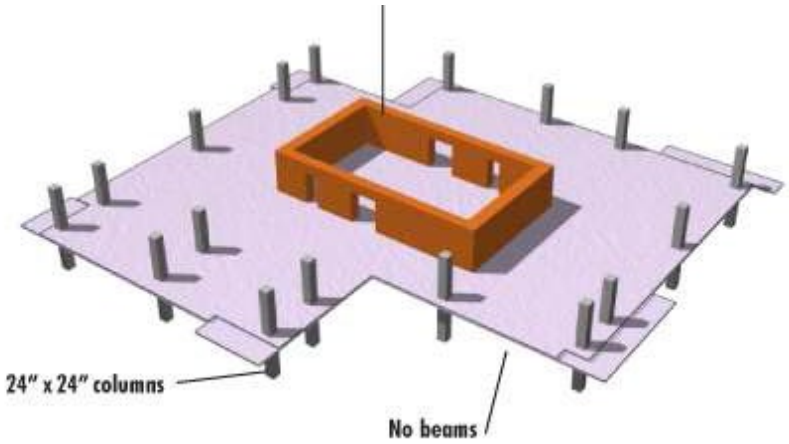
24" x 24" columns
No beams

The Home Insurance Building – Chicago, IL, 1885,
an early skyscraper

Figure 6.4, The 12-story Home Insurance Building (demolished in 1931) is considered to be the first skyscraper. A steel frame is the primary load bearing system in this building. There are also masonry infill walls that seal the building against the weather. Since the weight of the building is carried by the steel frame, the masonry walls are much thinner than is required to support such a tall building. The use of steel frame masonry infill walls was common in Los Angeles and San Francisco until the 1950's.

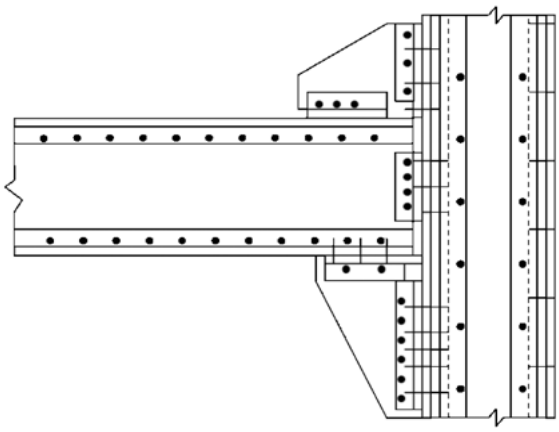

Figure 6.5. Typical early moment connection for steel frame buildings constructed prior to the 1950's. , consisting of heavy triangular
gusset plates, angles, and rivets connecting built-up columns and beams.

Steel frame buildings in downtown San Francisco performed well in the 1906 earthquake.

Homework Chapter 6

1. Assume that the base of a shear-beam (neglect bending deformations) with rigidity μ and density ρ is subject to tangential displacement that given by $u_x(t)$. Assume that the top of the shear beam is a free surface.

$$u_x(t) = \begin{Bmatrix} 0, & t < 0 \\ t, & t > 0 \end{Bmatrix}$$

a) Write the motion of the free end of the beam as a function of time.
b) Write the shear stress at the forced end of the beam as a function of time.
c) How would this problem change if you were to allow bending deformations in the beam?